ATLAS Internal Note
MUON-NO-155
22 April 1997

XTOMO2, Stereo-measurements of the MDT Muon Chambers using a High Precision X-Ray Tomograph

D.G.Drakoulakos, C.W.Fabjan,V.Falaleev, F.Lejal,
J.M.Maugain, S.Rangod, F.Rohrbach
CERN, Geneva, Switzerland

Z.V.Krumstein, Y.V.Sedykh, L.S.Vertogradov
JINR, Dubna, Russia

N. Benekos
NTUA, Athens, Greece

22 April 1997

(Presented to '96 ATLAS Muon Workshop)

Abstract

In this note the results of the second phase of the X-ray Tomography project, the so called **XTOMO2** are presented. A 600 mm long Tomograph was constructed to realize the stereomeasurements and to reconstuct the two-dimensional wire positions for different cross section of the MDT muon chambers. A 'reference triangle' was constucted for the calibration of the Tomograph. Furthermore, a 'tiltmeter' was installed to measure off-line the angular dispacement 'pitch'. A detailed comparison between the two scanning modes, i.e. the 'passive' and 'active', has been done and fast scanning algorithms have been developed to minimize the scanning time. An accuracy of less than 10 μm in the wire positions for both coordinates was achieved.

1 Introduction

The X-ray Tomography has been proposed as the tool for the mechanical and electrical quality control of the ATLAS Muon chambers. The main task of the project is to determine the precise location of the anode wires inside the Muon chambers by using X-ray measurement technics.

The measurements of the wire positions are done in two dimensions along a cross section of the chamber. This can be realised by 'stereo-measurements', i.e two separate measurements at the same chamber cross section with different X-ray inclination angles, the so called *scanning angles.*

For this propose, a general project working platform is planned until end of 1997 consisting of three phases (see fig.1). The results of the first phase - the so called XTOMO - was presented in [1], [2] and they played a major role in the prospective development of the project.

This note refers to the second phase of the project, the so called '**XTOMO2**', from the beginning up to September 96, when these results were presented on the First ATLAS Muon Workshop (Likithos, Greece). The milestones for the XTOMO2 were the following:

- The realization of the stereomeasurements.
- The optimization of the spatial accuracy of the X-ray tomograph.
- The minimization of the scanning time.
- The detailed comparison between different scanning modes, i.e. the 'active', 'passive' and 'semi-passive'.

This note is organized as follows:
The first two sections are set describing the fundamental concepts of the two-dimensional reconstruction of the wire positions using X-ray tomography. In particular, section 2 describes the developed principles and modes and section 3 desctribes the scanning method. Section 4 presents the technical description of the XTOMO2, section 5 describes the calibration procedure and the measurements for two MDT chambers, i.e. the Frascati/Cosenza and the Nikhef chamber and section 6 presents the conclusions.

2 Modes and principles of the X-ray tomography for MDT's.

The following three modes for measuring MDT chamber wire positions by using continious spectrum X-ray beam have been developed.

1. The 'passive' mode is based on the conventional principle for many X-ray applications, i.e. exploiting the significant X-ray absorption contrast between different materials.

2. The 'active' mode is based on X-ray photoelectric emission principle (XPE).

3. The 'semi-passive' mode (see section 2.3).

2.1 Passive mode.

This principle is based on the absorption difference between the aluminium of the tubes (thickness of 0.4 mm) and the gold plated tungsten of the anode wires (diameter of 0.05 mm). Indeed, using a well collimated X-ray beam - which moves along the face of a cross section of the tube - and a scintillator counter which detects the X-ray photons, we are able to record the shadow diagram of the tube.

Fig.2 shows the basic set-up for the passive mode and fig.3 presents the simulated single tube shadow diagram using a collimated X-ray beam of 0.04 mm width which produced from a **W** target [5].

2.2 Active mode.

This mode is based on the position dependent efficiency of pressurised cylindrical counters for X-rays. When the X-ray beam hits the wire photoelectrons and secondary processes, i.e. Auger electrons and fluorensence X-rays, are produced. Those have a significant propability to escape from the wire and be detect by the gas directly. As a consequence we exploit this excess of counting pulses to localize the position of the wire. Certainly, the background - counting rate due to aluminium tube, gas and electronic noise - has to be kept low [1].

Fig.4 shows the basic set-up for the active mode and fig.5 presents the simulated tube response using a collimated continuous spectrum X-ray beam of 0.04 mm width which is produced from a **W** target [5].

2.3 Semi-passive mode.

In this mode, although the chamber operates as in the active mode, the location of the wires are measured by using the scintillator system as in the passive mode. The advantage is that the position of the wires under real electrical environment are measured. This mode is a compromise between active and passive mode when static and dynamic distortions of the electric field could change the wire positions.

3 Scanning method.

The muon chambers consist of two myltilayers and each of them from three or four layers of tubes. Fig.6 shows the geometrical configuration of the muon chambers. Two independent scans (stereo-measurements) have to be done for the 2-dimensional mapping of the wire positions.

The stereo-measuring is realised by installing two fixed X-ray beam systems with different scanning angle on a linear scanner which moves parallel to the chamber cross section and takes advantage of the 'inclined projection principle' (described below).

3.1 Reconctruction of the wire cooordinates.

Fig.7 shows the schematic configuration of the measuring procedure. For every wire two measurements x_1, x_2 of the 'linear scanning position of the wire signal' - in the following referred to as l.s.p. - under two different scanning angles θ_1, θ_2 are realised.

The X, Z wire coordinates are expressed as:

$$X = \frac{x_2 tan\theta_1 - x_1 tan\theta_2}{tan\theta_1 - tan\theta_2}; \qquad Z = \frac{(x_2 - x_1)}{tan\theta_1 - tan\theta_2} \tag{1}$$

Futhermore, the following two systematic errors in both coordinates are involved:

- the l.s.p error Δx.
- the scanning angle error $\Delta\theta$.

Applying error analysis into eq.(1) results to:

$$(\Delta X)^2 = \frac{tan^2\theta_1 + tan^2\theta_2}{(tan\theta_1 - tan\theta_2)^2}(\Delta x)^2 + \frac{Z^2}{(tan\theta_1 - tan\theta_2)^2}(\frac{tan^2\theta_2}{cos^4\theta_1} + \frac{tan^2\theta_1}{cos^4\theta_2})(\Delta\theta)^2 \tag{2}$$

$$(\Delta Z)^2 = \frac{2}{(tan\theta_1 - tan\theta_2)^2}(\Delta x)^2 + \frac{Z^2}{(tan\theta_1 - tan\theta_2)^2}(\frac{1}{cos^4\theta_1} + \frac{1}{cos^4\theta_2})(\Delta\theta)^2 \tag{3}$$

If $\theta_1 = -\theta_2 = \theta$ then eq. (2) and (3) result to:

$$(\Delta X)^2 = \frac{1}{2}[(\Delta x)^2 + \frac{Z^2}{cos^4\theta}(\Delta\theta)^2] \tag{4}$$

$$(\Delta Z)^2 = \frac{1}{2tan^2\theta}[(\Delta x)^2 + \frac{Z^2}{cos^4\theta}(\Delta\theta)^2] = (\frac{\Delta X}{tan\theta})^2 \tag{5}$$

3.2 Scanning Angles

The selection of the scanning angles was the most important subject under consideration for two reasons:

- They define the 2D accuracy of the wires position (see eq. (2) - (5)).
- They depend on the chamber structure characteristics (see fig.6), i.e. the height of the spacer, the symmetry between the two multilayers, the number of the layers of each chamber (6-fold or 8-fold) and the horizontal/vertical wire pitch.

The selection for the optimal set of the scanning angles was realised by a simulation program for pattern reconstruction of the wire and tube positions of various type of chambers and analytical calculations using the geometrical parameters of the chambers. The detailed presentation of this work including the Monte Carlo for XTOMO2 is described in [5]. The conclusions of this investigation are summarized in the following scanning angles definition criteria:

1. Avoiding the wire-wire(s) and the wire-tangent tube wall(s) overlaps.
2. The accuracy of the 2D wires reconstruction should be less than 0.01 mm.
3. Compatible with the construction design and Muon pattern recognition constraints.
4. Significant recognition of the wires and identical pattern recostruction for various chamber types i.e BL, BM, etc.
5. Maximization of the scanning area.
6. Mechanical stability of the 'scanning head'.

An optimum set of scanning angles that fulfils all the above mentioned criteria is $\theta_1 \approx 31^o$, $\theta_2 \approx -31^o$ in respect to the z-axis.

4 Technical Description

The schematic presentation of the **XTOMO2** can be seen on the fig.8. The supporting bridge of the scanner was installed in the middle of a heavy iron table. The set up of the bridge on the iron table and the instalation of the 600 mm long linear positioning stage[1] on the bridge was similar to the one in XTOMO [2]. The 'scanning head' is mounted on the scanner carrier using two supporting reference pins. In the following paragraphs there is a detailed descriprion of the XTOMO2 components.

4.1 Scanning Head.

Fig. 9 shows the design of the 2D scanning head. On the top of the aluminium plate two X-ray beams systems were mounted with inclination angles of 31^o and -31^o respectively. Every X-ray system consist of a X-ray shielded tube [2], a small linear stage [3] and a X-ray collimating system. The collimating system consist of a 350 mm long a rail fixed to the aluminium plate, two tungsten beam collimators C1 and C3 with slit dimensions 0.03×10 mm^2 and a schielding collimator C2 with slit dimensions 3×10 mm^2. The aluminium bases of these collimators could be moved along the rail. A shielding from aluminiun-lead foils cover all the collimating system, thus avoiding leakage radiation. *Both X-ray beam collimators C1 and C3 define the beam axis and the scanning angle (in respect to the z-axis).* The X-ray tube is connected with a 6 m long cable to the power supply and emits continuous spectrum from a **W** target, the so called *focus spot*, with dimensions 0.04×12 mm^2 at 6^o take-out angle through a berillium window.

The X-ray tube was mounted to the small linear stage on the aluminium plate. Futhermore, the small linear stage was able to move in such way that the take-out angle in respect to beam axis was 3^o [1]. Under such configuration the projective image of the target along the beam axis was 0.02×12 mm^2.

4.2 Detector of the X-ray quanta and Electronics.

The detection system depends on the operating mode.

For the passive mode, a plastic scintilator with dimensions $800 \times 80 \times 30$ mm^3 is installed. Futhermore, two photomultiplayers are installed at both ends of the scintillator and read in coincidence at first to reduce the noise to signal ratio to less than 1 % and second to maximize the efficiency of the detector (attenuation effect). A CAMAC crate with an interface to a 486 PC is used for the data acquisition system. The signals from both PM's are shaped by a discriminator and selected by a coicidence unit. After that, the digital signals are driven to a PC scaler card[4].

[1] ATS5000, production of AEROTECH firm, USA.
[2] PW 2214/20 Production of PHILIPS, Netherland.
[3] ATS0300 production of AEROTECH firm, USA, [3].
[4] AT-M10-16E-2, NATIONAL INSTRUMENTS firm.

For the active mode the detection system were the cylindrical drift tubes of the chamber itself. The amplified signals from all individual tubes were separately sellected and shaped by two dicriminator units in the set of 16 tubes. Afterwards the signals for every layer of the chamber are selected in one output by using OR ports and are driven to a PC scaler card[5]. Fig.10 and fig.11 present the read-out organization for the passive and active modes respectively.

4.3 Software.

The operation program written in C language consists of the 'scanning algorithm' and the 'data storing loop'. The scanning algorithm defined the motion of the linear scanner by using programming commands of the PC bus motion controler[6]. The control of the data storing loop was realised with the PC timer (with time error of 20 μs) which set the sychronization between the scanner and the detection system as well as the data storage.

Three data parameters are recorded on-line:

- The scanner position X in millimeters.
- The counted photons I from the scaler. In the case of the active mode every layer k corresponds to a scaler I_k.
- The counting duration T in microseconds

Four scanning operation programs were used corresponding to the various scanning modes:

- **Flying 1** (old SCAN3): The scanner moved along the whole scanning length L with constant velosity $v_s = 0.5$ mm/s. The scaler(s) was active during the scanner movement. The data parameters are recorded in the output file every 20 or 10 μm. For a scanning length L = 600 mm the scanning time was $t_s = L/v_s = 20$ minutes.
- **Stepped 1:** The scanner moved with constant velosity $v_s = 0.5$ mm/s for a length s=0.01 mm and stops for a time interval T=0.04 sec repeatedly. The scale counted only at this time interval. For a scanning length L=600 mm, the scanning time was $t_s = L * (1/v_s + T/s) = 60$ minutes.
- **Stepped 2** (old SCAN5): This operation program exploits the periodicity of the wires inside the chamber. The scanning cycle is the same as the 'stepped 1' but in the region where there are no wires ($L_o \approx 2/3 * L$) the scanner moves with speed $v_o = 10 * v_s$ without stopping and storing data. The scanning time was $t_s = (L - L_o)(1/v_s + T/s) + (L_o/v_o) = 21.3$ minutes.

[5]AX5216, 5 channel counter, AXIOM firm.
[6]UNIDEX 500, AEROTECH firm, USA.

- **Flying 2** The scanner moves with constant velosity v_s in the wire region and with speed $v_o = 10 * v_s$ elsewhere without stopping. The scanning time was $t_s = (L - L_o) * 1/v_s + (L_o/v_o) = 8$ minutes.

  This operation program wasn't installed due to the fact that the PC interface couldn't negotiate such a fast scanning algorithm. This program should be kept as a future option when a VME interface will be installed.

Fig.12 shows the configuration of the scanning operation programs (described above).

4.4 Analysis

The analysis program has been written in the COMIS Fortran interpreter under the PAW environment. The main steps subroutines of the analysis program are:

- Finding the wires signals - peaks and dips for the active and passive mode respectively. For this purpose first and second derivative algorithms are used (see paragraphs 5.3 and 5.4).
- Defining suitable initial parameters for the fit procedure of the wire signals (see paragraphs 5.3 and 5.4). The sum of a gaussian for the signal and a linear form for the background (5 parameters in total) was used for the fit.
- Fitting the wire signal (5 fit parameters) and finding the two l.s.p for each wire (see paragraphs 5.3 and 5.4).
- Correcting the l.s.p by using data for three linear stage parameters, i.e. linear position, straigthness and pitch, (see paragraph 5.2.1).
- Determination - from the 'reference triangle' measurements (see paragraph 5.2.2) - of the scanning angles θ_1, θ_2 and the corresponding errors $\Delta\theta_1$ and $\Delta\theta_2$ using the MINUIT fitting package.
- Two-dimensional wire reconstruction (see paragraphs 5.3 and 5.4).

In fig.13 the logical diagram of the analysis program is shown.

5 Measurements.

An alingment procedure of the XTOMO2 is carried out before measuring the chambers. Afterwards, the calibration procedure from which the scanning angles are found, is done.

The measurements have been performed on two chambers, i.e. the Frascati/Cosenza 8-layer chamber using only the passive mode and the Nikhef 4-layer chamber with both the passive and active modes.

5.1 Alignment-procedure

The alingment procedure was extermely critical for the final accuracy of the XTOMO2. It has be done in the following steps:

- The alignment of the X-ray target in respect to the beam axis - defined by the two beam collimators C1 and C3 (see fig.8) - has been achieved by moving the X-ray tube's small linear stage with a step of 2 μm .The 'stepped 1' program was installed under the LabView framework. The quanta of the X-ray beam in each position are measured from a plastic scintillator. Fig.14 shows the scintillator counts as a function of the position of the X-ray tube. Afterwards the X-ray tube is fixed at the linear stage position of the maximum intensity.

- The X-ray beam profile is measured by using dental X-ray films (see fig.15). The dimension of the beam is measured to be 5×0.04 mm^2 and the beam divergence is 150 μrad . For the measurements of the X-ray beam energy spectrum a silicon pixel detector[7] is installed.

- The CERN Survey group adjusted the orthogonality of the XTOMO2 with an accuracy of less than 0.5 mrad.

- For the alignment of the Nikhef chamber and the reference systems, i.e. 'ruler' and 'triangle', a precise aluminium table - see fig.8 - with three adjustable micrometer pivots was constructed[8].

5.2 Calibration procedure.

The XTOMO2 calibration procedure had the following two aims:

- the minimization of the l.s.p. error Δx (see eqs. (4) and (5)) and

- the determination of the scanning angles θ_1 and θ_2 and their corresponding errors $\Delta\theta_1$ and $\Delta\theta_2$ respectively (see eqs. (4) and (5)).

The final goal was to reconstruct the wire position in the XZ plane with an accuracy of less than 10 μm.

[7]Thanks to Dr.P.Wielhammer

[8]Thanks to Mr.M.Fillion

5.2.1 The linear scanning position error

The (l.s.p.) error is consists of the 'fit error' and the 'linear stage error'. The fit error is found to be 1 μm by measuring a reference ruler composed of 20 wires [2]. The linear stage error mainly is affected by the following three parameters:

- the linear position accuracy[9] $\Delta x_L = \pm 5^*$ μm
- the straightness accuracy $\Delta z_S = \pm 3^*$ μm
- the angular displacement 'pitch' (rotation of the linear stage carrier in XZ plane) accuracy $\Delta \theta_p = 70^*$ μrad

Calibration curves for the linear position and the straightness - in the X-ray beams working plane - were provided from the company with repeatability less than 1 μm and are shown in fig.16.

Furthermore a 'tiltmeter'[10] with accuracy 1* μrad is installed on the XTOMO2 for the measurements of the angular dispacement 'pitch'. In fig.17 the value of the 'pitch' as a function of the scanning coordinate is shown. The 'pitch' repeatability was measured to be less than 1 μrad at full scanner length.

Afterwards, the l.s.p. error Δx is determined to be 2 μm.

5.2.2 Calibration of the scanning angles

The calibration of the scanning angles has been realised with a device, hereafter called **reference triangle**. It consists of 3 gold plated tungsten wires of 50 μm diameter. The wires are fixed carefully on the edges of an aluminium triangle frame, which is almost isoscele. Fig.18 shows the schematic design of the 'reference triangle'.

A highly accurate optical scanner[11] measured the sides of the triangle - which are defined by the wire dintances - equal to $d_{12} = 388.393$ mm, $d_{13} = 388.311$ mm and $d_{23} = 399.925$ mm with an error of $\Delta d^o = \pm 3^*$ μm.

Afterwards, it is installed on the XTOMO2 and is aligned parallel to X-ray beams plane with high accuracy using the alignment table. It is scanned with the passive method from both X-ray beams.

For the determination of the scanning angles the following methodic is applied:

1. Six l.s.p (two for every wire i, x_{i1} and x_{i2}) are determined using the analysis software as described in paragraph 4.4.

2. A gaussian generator with an r.m.s. of 2 μm generates the errors Δx_{i1} and Δx_{i2} of the l.s.p for each wire i.

[9] It is important to mention that in the micro-mechanics terminology the 'accurary' is defined as the maximum deviation between actual and theoretical position value - in the physics terminology it would correspond to 3σ deviation - and the 'repeatability' is defined as the standard deviation of the actual position when the measurements are repeated [4]. From now on, an asterics above the parameter value will indicate when the micro-mechanics terminology is used.

[10] Production of LEICA firm, Germany.

[11] Thanks to Mr.C.Boudineau, Metrology group, CERN.

3. Using the eq. (1) the X_i^t and Z_i^t are defined as:

$$X_i^t = \frac{(x_{i2} + \Delta x_{i2})tan\theta_1 - (x_{i1} + \Delta x_{i1})tan\theta_2}{tan\theta_1 - tan\theta_2} \tag{6}$$

$$Z_i^t = \frac{(x_i 2 - x_i 1 + \Delta x_{i2} - \Delta x_{i1})}{tan\theta_1 - tan\theta_2} \tag{7}$$

Afterwards, the distance between i and j wires, d_{ij}^t, measured with the tomograph is expressed as:

$$d_{ij}^t = \sqrt{(X_j^t - X_i^t)^2 + (Z_j^t - Z_i^t)^2} \quad i,j = 1,3 \tag{8}$$

Therefore, in eq. (8) the scanning angles are the unkwown variables.

4. A gaussian generator with an r.m.s. of 1.5 μm gives the distance errors between i and j wire, Δd_{ij}^o, for the optical measurements and the corresponding (optical) distances are define as:

$$d_{ij}^o = d_{ij} + \Delta d_{ij}^o \quad i,j = 1,3 \tag{9}$$

5. The function minimization and error analysis package MINUIT is used to determine the scanning angles and their corresponded errors by minimising the following expression:

$$\sum_{k=1}^{n} (d_{12}^t - d_{12}^o)^2 + (d_{23}^t - d_{23}^o)^2 + (d_{31}^t - d_{31}^o)^2 \tag{10}$$

where n is equal to 300.

From the calibration procedure the scanning angles are determined as:

- $\theta_1 = (31.01516^o \pm 0.00048^o)$
- $\theta_2 = (30.88025^o \pm 0.00047^o)$

Fig.11 shows the results of the scanning angles calibration. In addition, the Monte Carlo program agreed with the results of the calibration procedure.

5.3 Measuring the Frascati-Cosenza chamber.

The chamber is scanned only in passive mode. In Table 1 of Appendix 1 the scanning parameters are shown. In fig.20 the dark tubes represent the 2-dimensional scanning region of the chamber. Five broken wires are detected - black tubes - and 18 non-recostracted wires - dark grey - due to the effect of the aluminium spacer. Fig.21 shows the counts per step as a function of the X-coordinate in the region where a broken wire is recognized and fig.22 in the region where the aluminium spacer affects

the counting rate. For the wires recognition the second derivative of the counts is used. Fig.23 presents the effect of the wire-finder algorithm on the counting rate. The two-dimensional wire positions are presented in table 3 of Appendix 1 and the image reconstruction of the scanned wires in fig.24. The mean value of the horizontal wires pitch is found to be 30.05 mm (see fig.24 top) which is in agreement with the consrtuction properties of the chamber.

5.4 Measuring the Nikhef chamber.

The small Nikhef chamber is measured with both passive and active mode. The scanning parameters are shown in table 1 of Appendix 1. Fig.25 shows the X-ray counts detected from a plastic scintillator (passive) For the measurements of the Nikhef chamber, the stepped 2 scanning program is used. Fig.26 shows the X-ray counting rate detected from different layer tubes (active method) and fig.27 shows the shadow diagram for the semi-passive mode. The first derivative of the counts is used as wire recognition algorithm (see fig.30 for the passive and fig.31 for the active method).

In fig.28 and fig.29 the fit procedure of the wires signals for passive and active modes respectively is presented. In table 2 of Appendix 1 the reconstruted two-dimensional wire positions for active and passive methods are presented. Fig.32 and 33 shows the distribution of the distance differences between neighbouring wires in the same layer for the passive and active method respectively. The mean value of the horizontal wire pitch is found to be 30.01 mm which is consistent with the construction properties, with r.m.s. of 44.91 μm (active) and 45.35 μm (passive). Fig.34 shows the two-dimensional wire reconstruction for each layer and a displacement of 300 μm in the Z-coordinate for the fifth wire in the second layer is seen.

6 Conclusion

In this work the stereo-measurements of two chambers are realised.

For the calibration procedure a 'reference triangle' is used which gives excellent results in the final spatial accuracy of the XTOMO2, i.e. an accuracy less than 10 μm in both coordinates is achieved. Furthermore, calibration data of the 'linear position' and 'straightness' provided by the company and from off-line measurements of the angular 'pitch' is used.

Fast operation scanning programs are written to minimize the scanning duration (i.e. 'stepped 2'). The scanning duration was limited from the following items:

- The MS-DOS mainframe of the 486 PC was not adequate for the sychronization between the scanner motion and the measured parameters down to 10 Hz, i.e. 100 msec per measured point. For this reason a VME controller is proposed in order to reduce the scanning duration of the X-ray tomograph significantly.
- The off-line calibration procedure (reference systems installation and measurement).
- The off-line mechanical control system increase the scanning duration. Due to the high quality of the linear stage, i.e. the linear stage repeatability was 1 μm, only the 'pitch' parameter is measured.

  If the repeatability of the scanner was modest (it was not the case) it would have also affected the reliability of the calibration procedure dramatically and consequently also the accuracy of the tomograph.

Therefore, high reliability, high accuracy and short scanning time of the tomograph device implies:

- On-line measurements with a presice mechanical control system for the 'linear position', 'straigtness' and 'pitch' parameters at the X-ray beams working plane.
- On-line measurements of the 'reference system' which consists of 2-level set of tungsten wires which cover the whole scanning length.
- A VME interface for the data aquisition system which can handle fast scanning algorithms.

From the detailed comparison between active and passive mode, the following conclusion can be stated:

- The passive mode, which provides only mechanical control of the wire position of the muon chambers, is simpler than the active due to uncomplicated data aquisition system.

- No displacements of the wire positions due to the statical or dynamical distortions of the electric field are found (see fig.32 and fig.33).
- The active mode is the most efficient of the two, due to the following advantages:

    1. Better signal to background ratio (2:1) than the passive mode (0.6:1) due to the possibility to minimize the background of the gas using lower operating gas pressure (see fig.28 and fig.29) or adding a small fraction of an electronegative gas [1].
    2. Possibility to obtain electrical and mechanical response of all the individual tubes of the chamber.
    3. No lost wires due to the aluminium spacer frame. The operating high voltage of the X-ray generator is 55-60 kV for the active mode and 40-45 kV for the passive.

6.1 Acknowledgments

This work represents the second phase of the X-ray Tomography project from January to Semptember 1996. The results are presented at the First ATLAS Muon Workshop in Likithos (Greece).

It is a pleasure to acknowledge the support from many collaborators and assosiates in the realization of this work. In particular Dr. F. Linde, Prof. J.C. Susinno and Prof. B. Esposito for the their essensial support by providing MDT chambers to measure; the ECP team, M. Fillion, S. Greenwood, G. Acquistapace, A. Looten for the constructive technical support; Prof. H. Wellestein for his constructive suggestions about the reference triangle and the tiltmeter; Dr. I. Vichou for her corrections on preliminary versions of this note; Prof. M. Dris and Dr. J. Wotschack for their essential support during this phase of the project.

References

[1] G.D.Alexeev, I.Boyko, H.Breuker, G.Chelkov, D.G.Drakoulakos, C.W.Fabjan, M.Ignatenko, Z.Krumstein, Yu.Sedykh, L.Vertogradov, XTOMO, a Prototype of the X-ray Tomograph for High Presicion Measurements of the MDT Muon Chambers. ATLAS Internal Note, MUON-NO-142, March 1997.

[2] D.G.Drakoulakos, C.F.Fabjan, M.Ignatenko, Z.Krumstein, L.Vertogradov, XTOMO, one-dimensional X-ray Scanning of a 8-layer MDT Prototype using the 'Passive Mode'. ATLAS Internal Note, MUON-NO-151, April 1997.

[3] Catolog: 'AEROTECH Motion Control Product Guide', 1993.

[4] Catolog: 'MICRO-CONTROLE Product Guide', 1994.

[5] J.Berbiers, D.G.Drakoulakos, C.W.Fabjan et al., 'DiMiTriX, a Large X-ray Tomograph for Measururing of the MDT Muon Prototype Chambers', ATLAS Internal Note, under preparation.

Figures

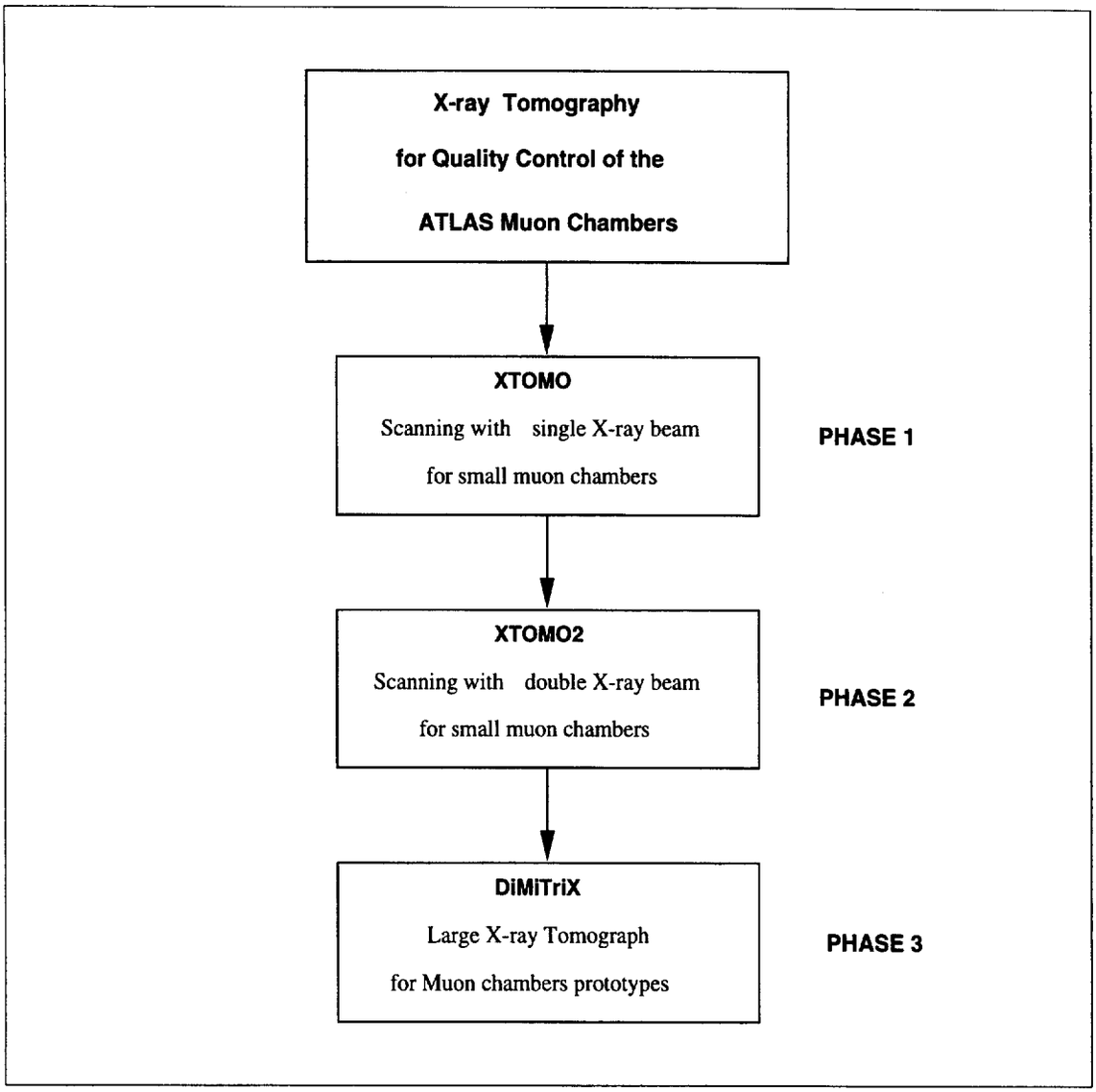

Figure 1: The working platform of the X-ray tomography project for the ATLAS Muon chambers.

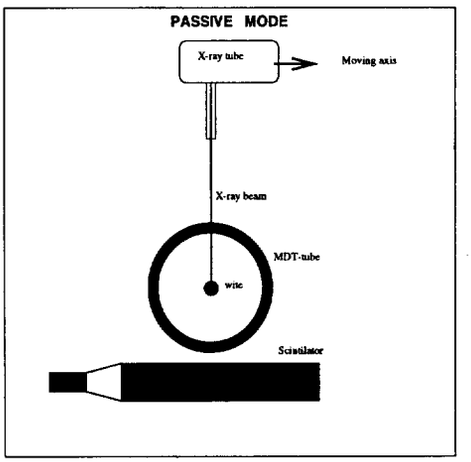

Figure 2: Passive mode: The basic set-up for a single drift tube.

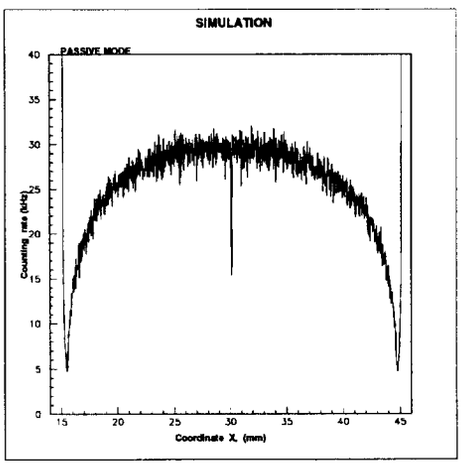

Figure 3: The simulated shadow diagram in a cross section of the tube.

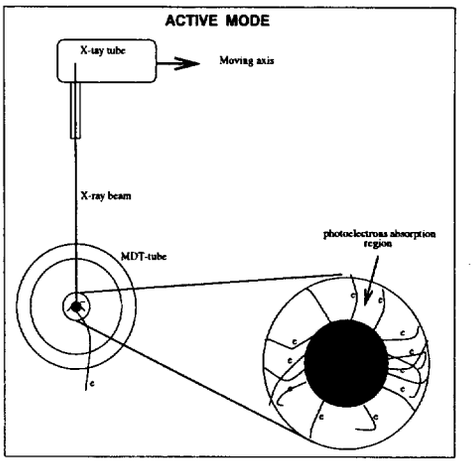

Figure 4: Active mode: The basic set-up for a single drift tube.

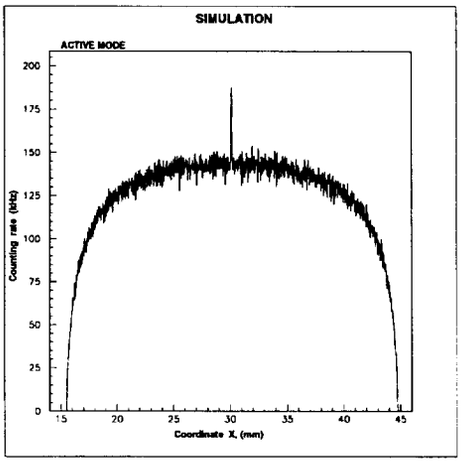

Figure 5: The simulated tube response for the active mode using a collimated X-ray beam of 0.04 width.

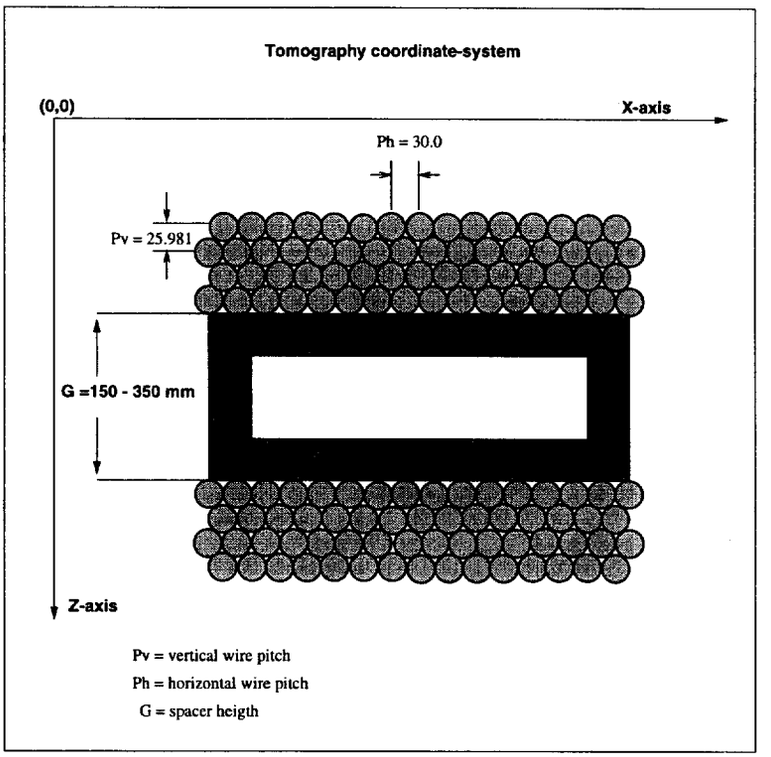

Figure 6: The schematic configuration of the MTD chambers and the X-ray tomography coordinates system.

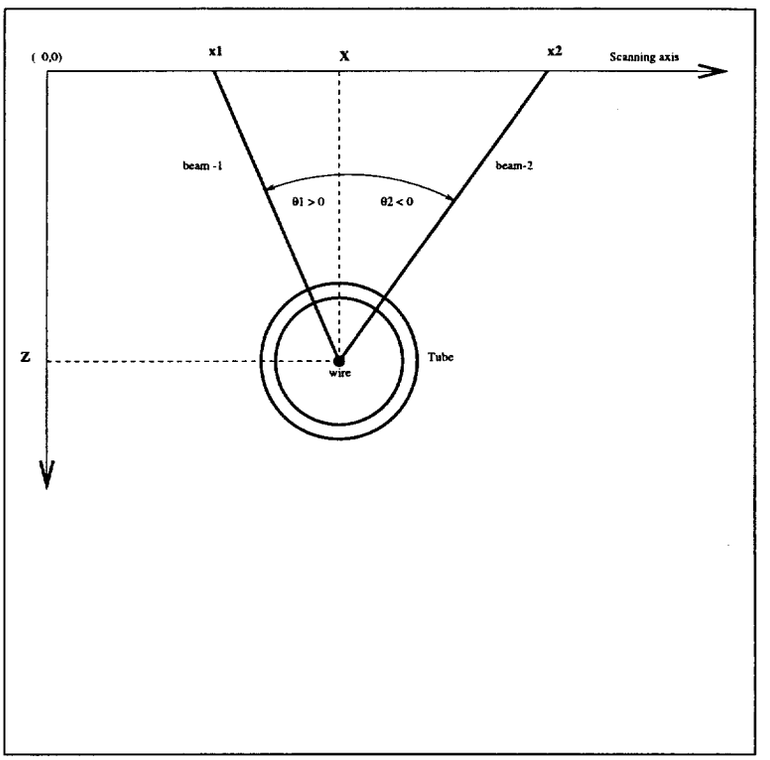

Figure 7: The schematic configuration of the stereo-measurements using two X-ray beam with different inclination angle.

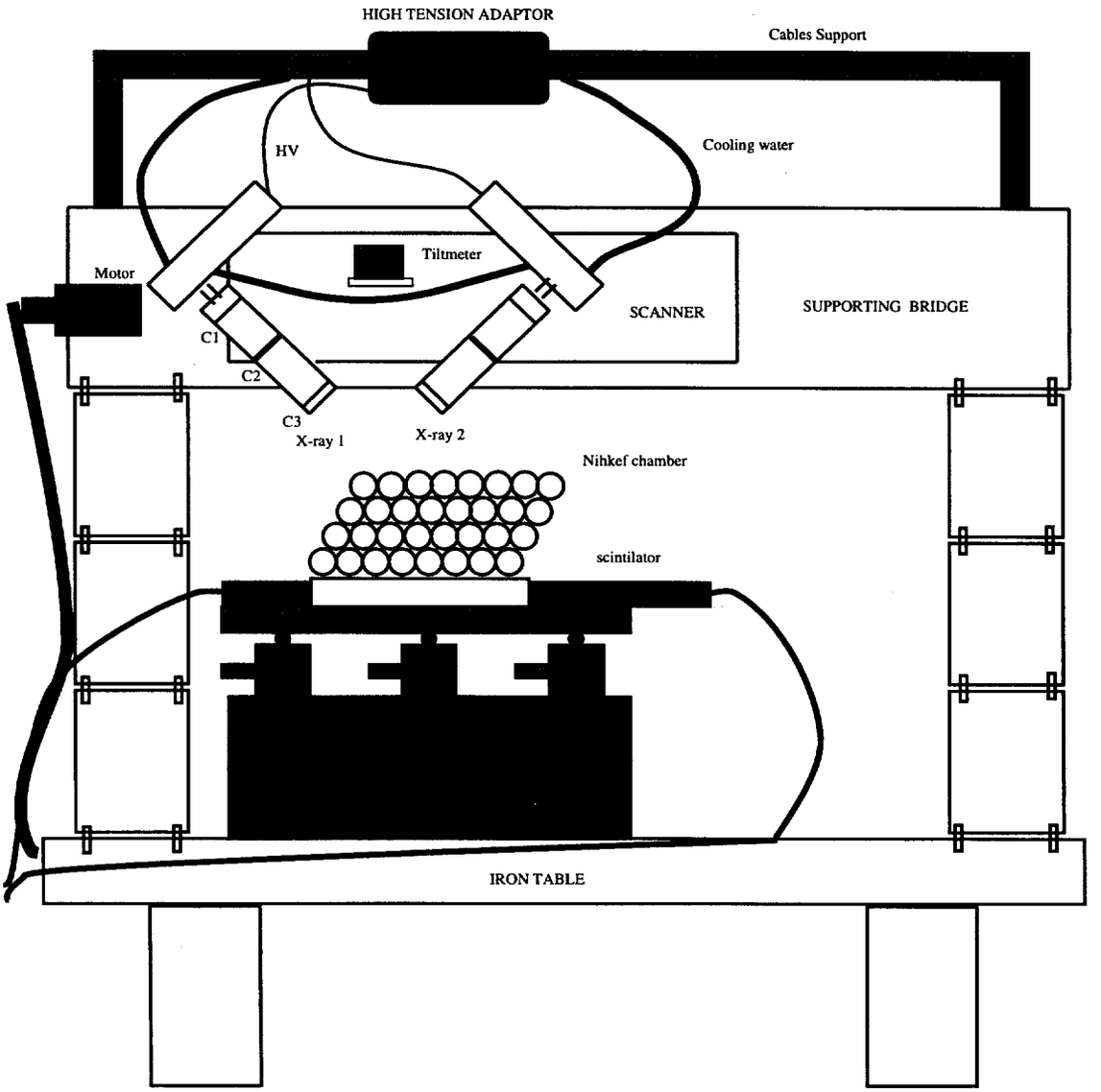

Figure 8: The X-ray Tomograph set-up for active and passive modes measurements.

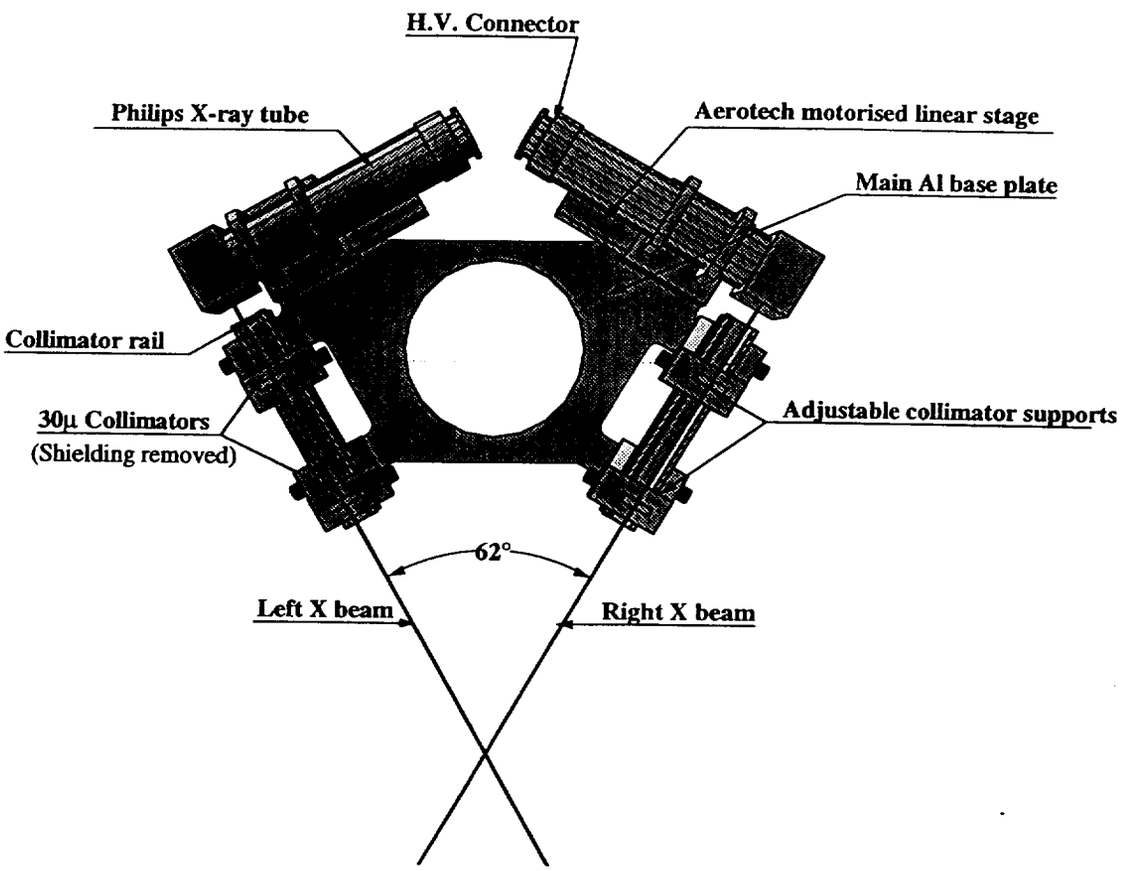

Figure 9: Design of the XTOMO2 scanning head .

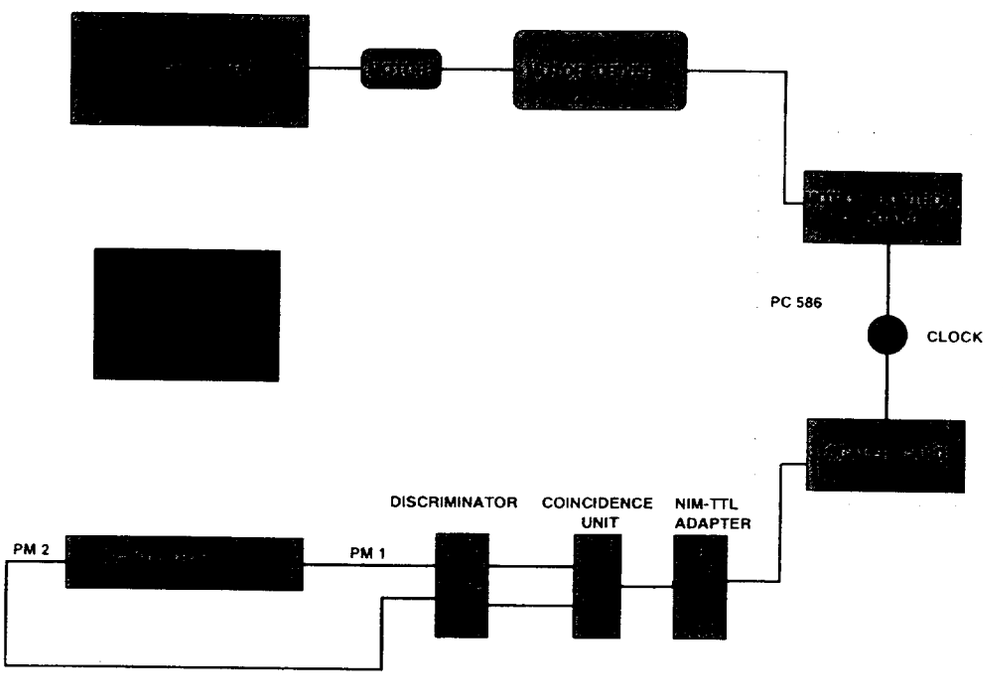

Figure 10: Read-out for the passive mode with which the Nikhef chamber and Frascati/Cosenza chamber are measured.

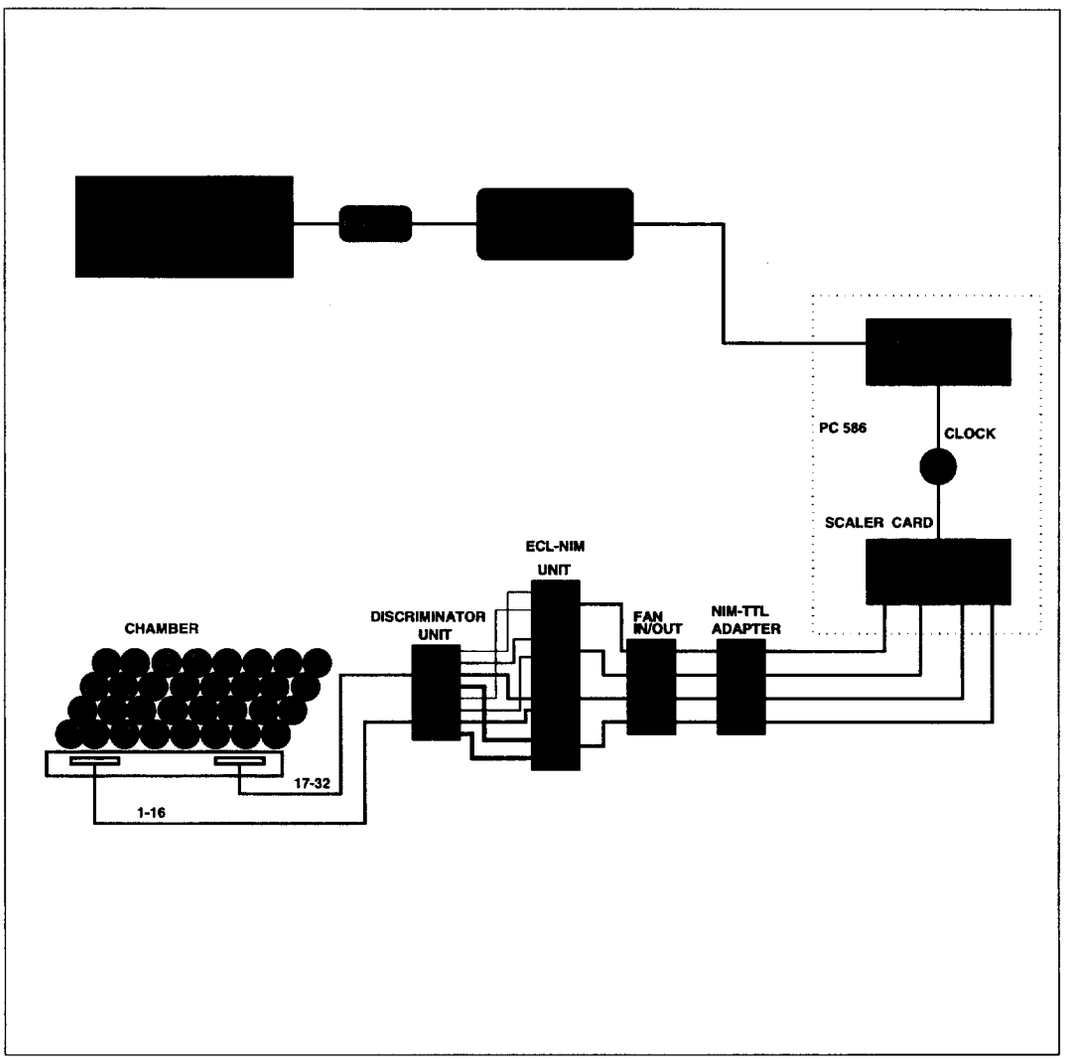

Figure 11: Read-out for the active mode with which the Nikhef chamber is measured.

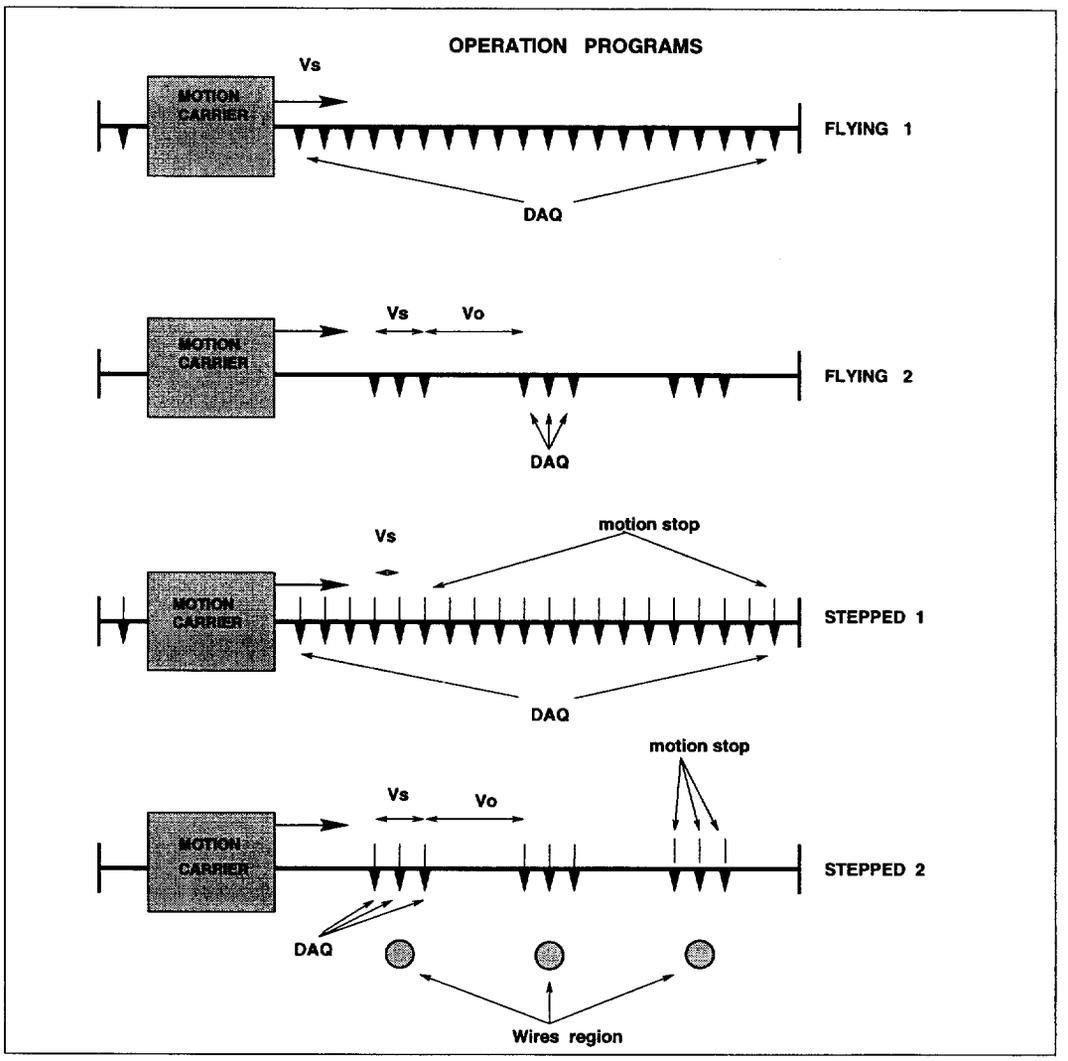

Figure 12: Schematic diagram of the four scanning programs.

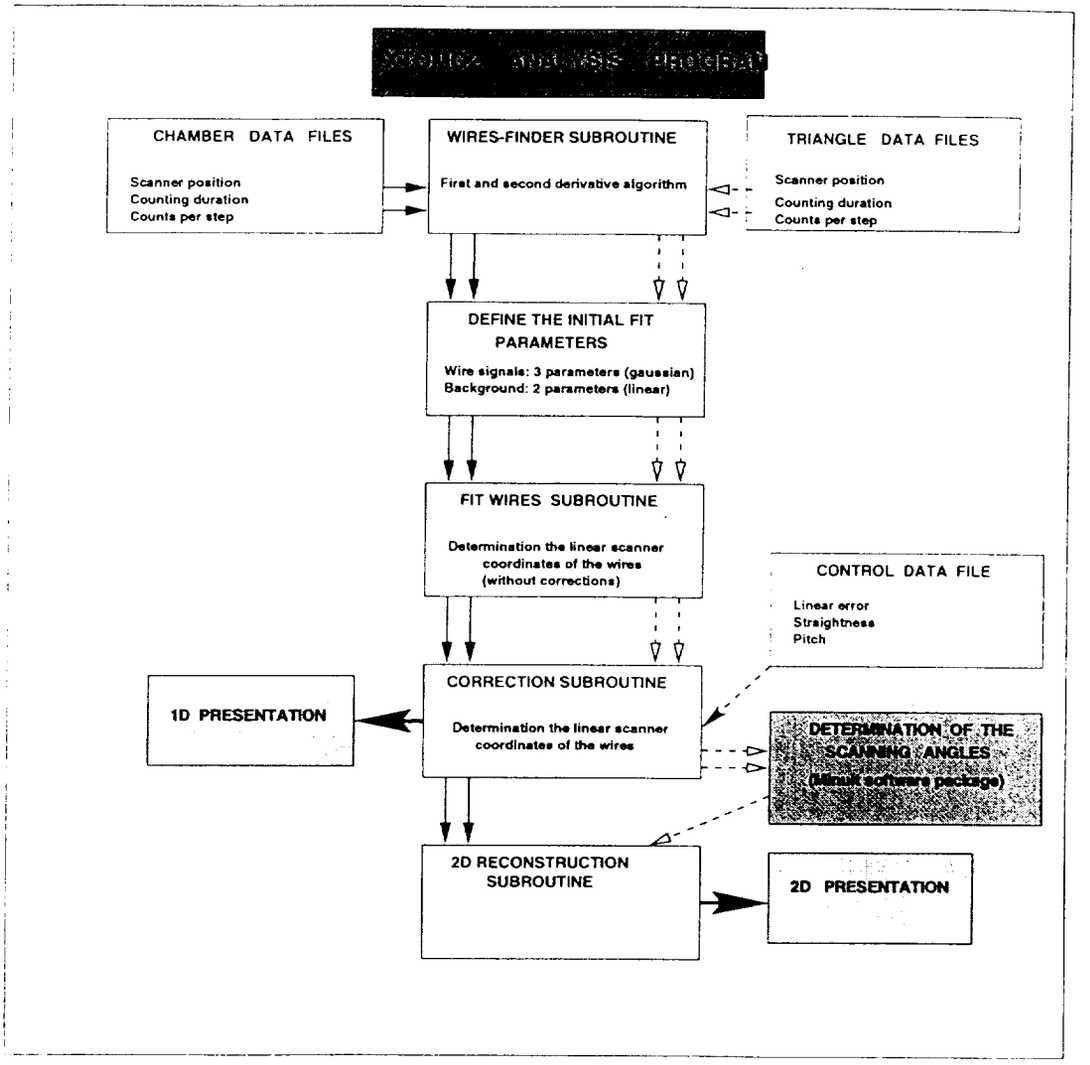

Figure 13: The block diagram of the analysis program.

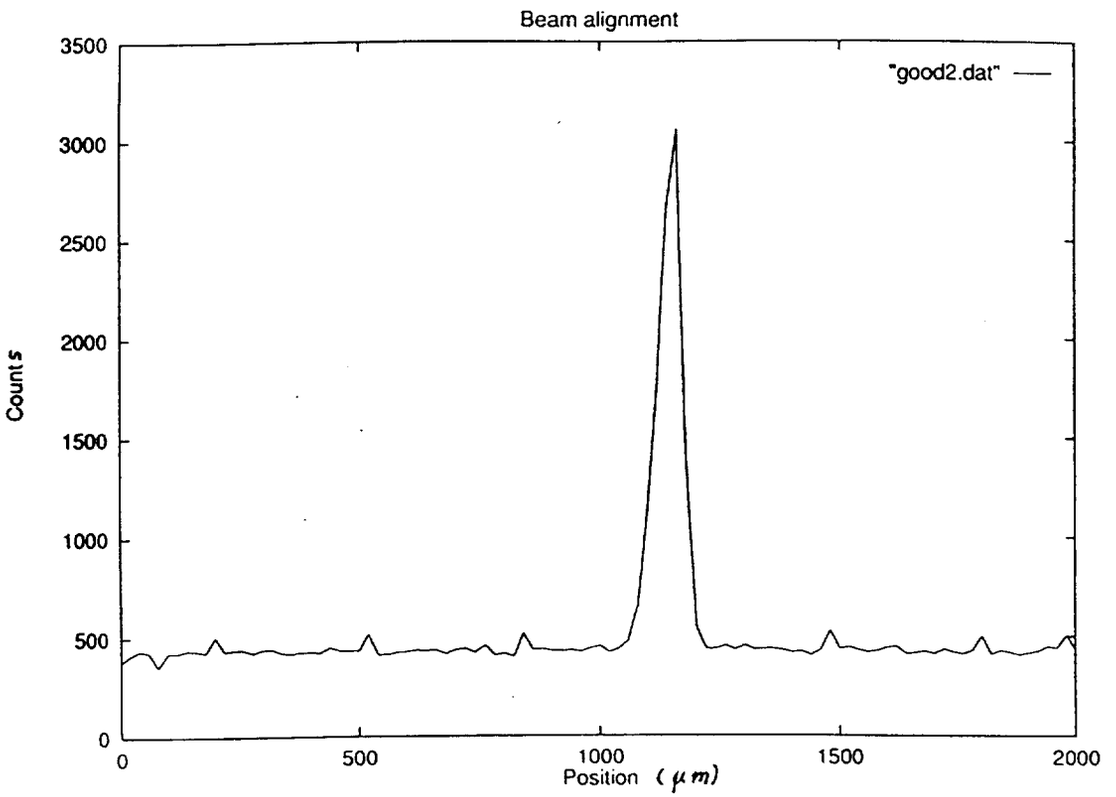

Figure 14: The counts per step as a function of the position of the X-ray tube, demostrating the alignment of the X-ray target with respect to the beam axis.

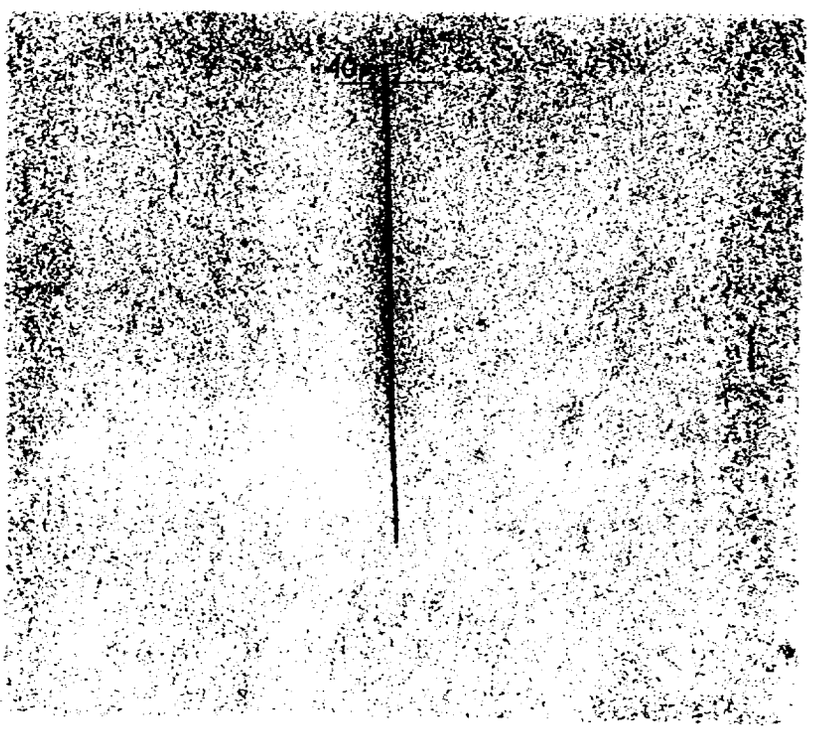

Figure 15: Spatial profile of the X-ray beams measured with dental X-ray films.

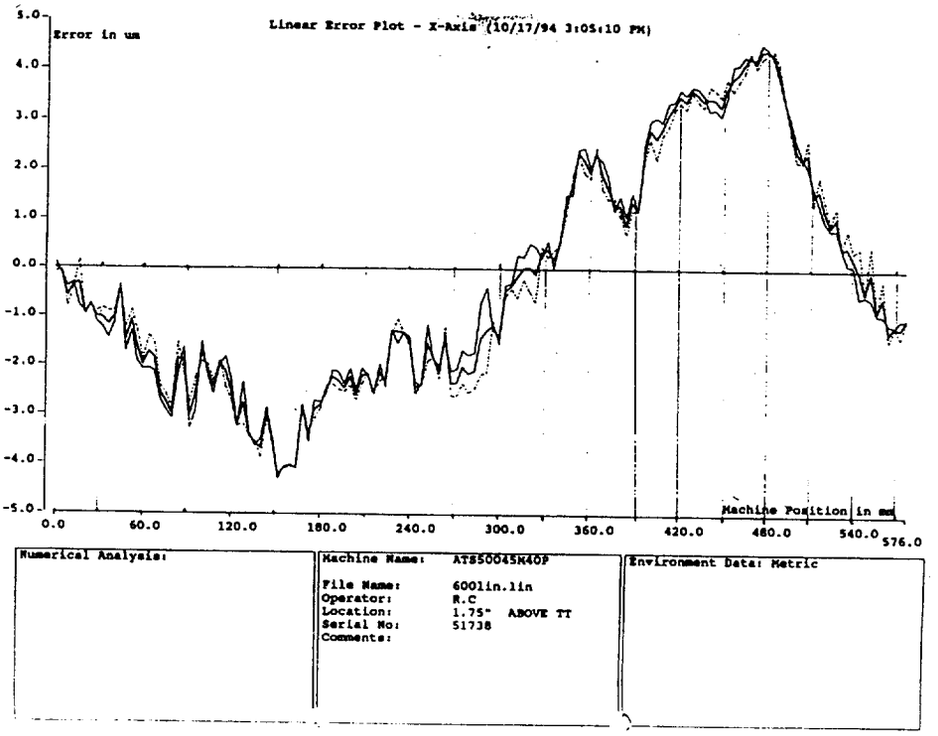

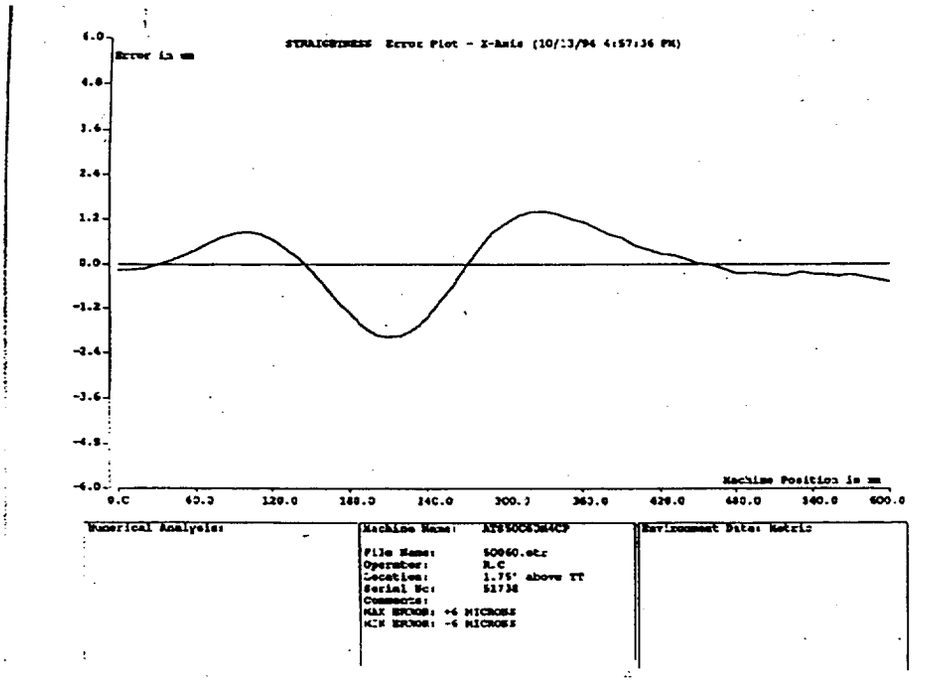

Figure 16: Calibration curves for 'linear position' and 'straigthnes' provided from the company.

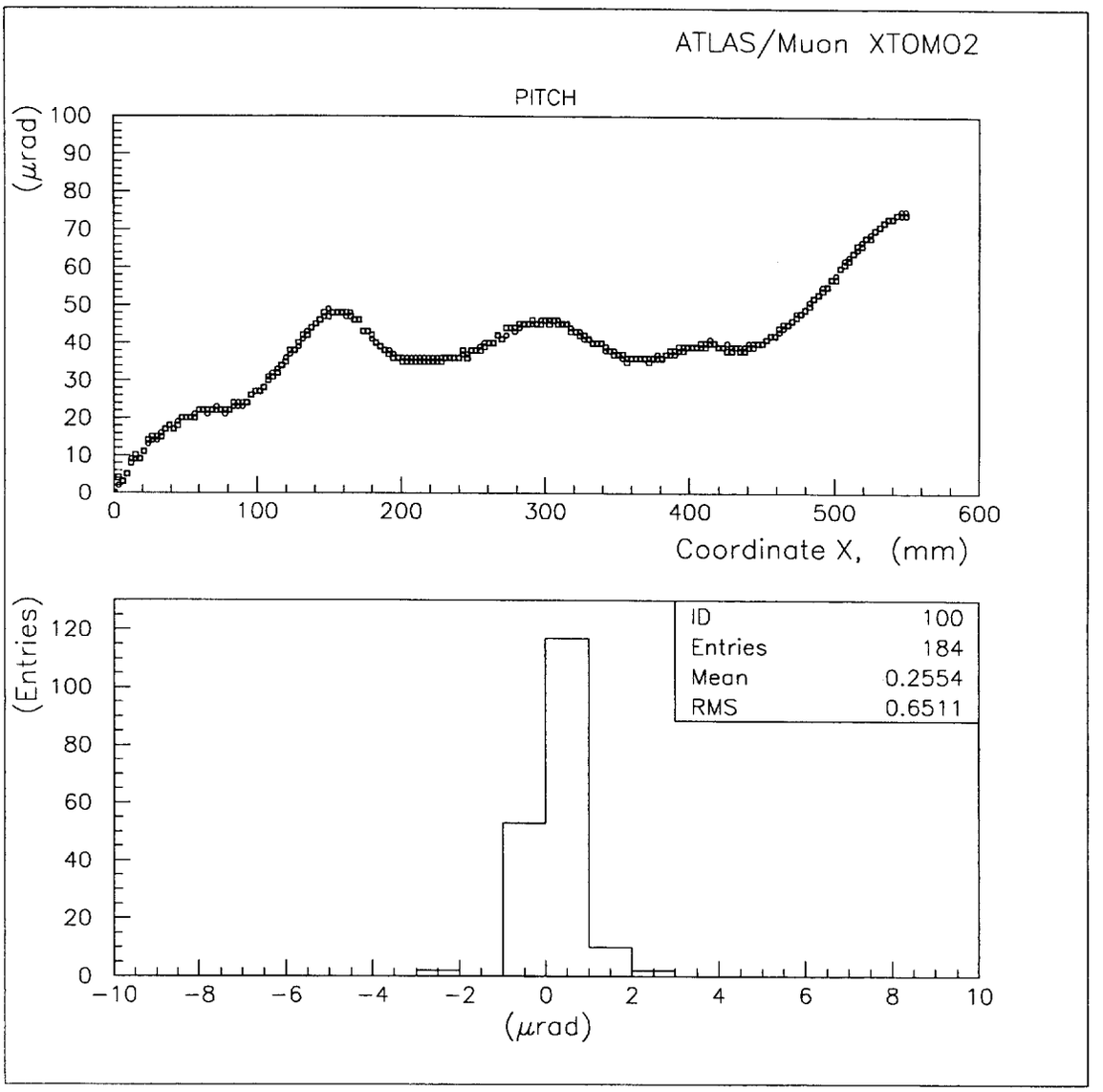

Figure 17: The pitch as a function of the scanner position.

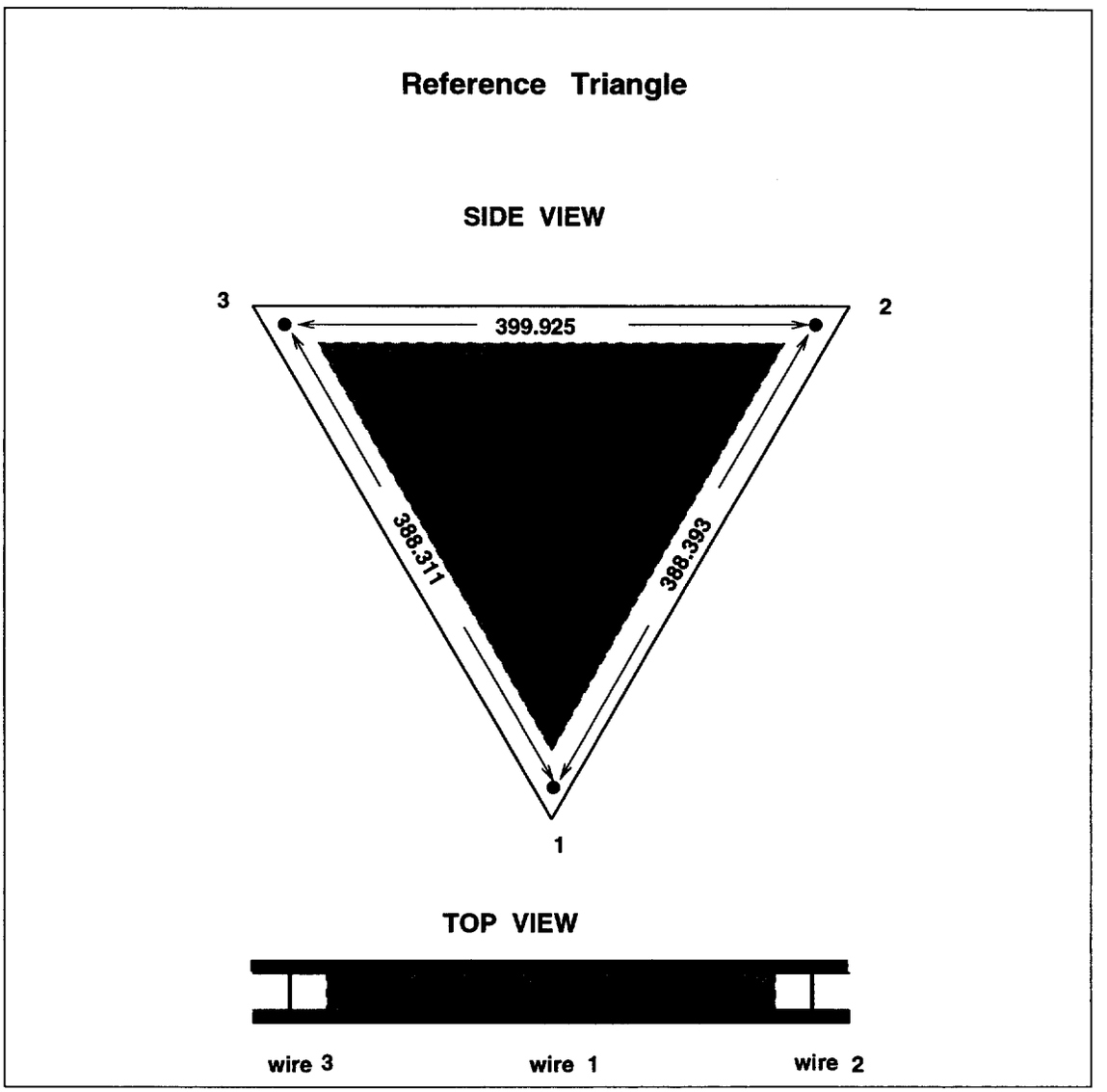

Figure 18: The 'reference triangle' configuration.

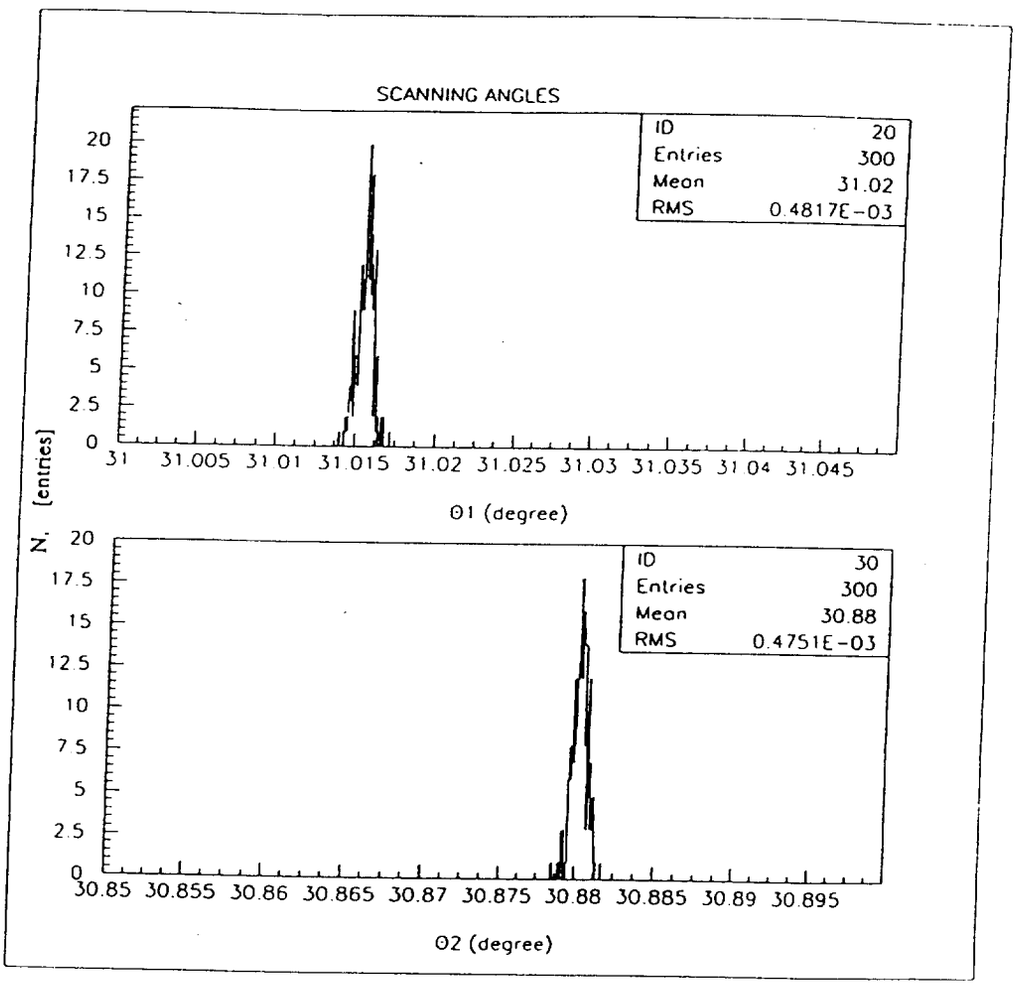

Figure 19: The results of the calibration procedure for the scanning angles, found to be $\theta_1 = 30.01516^o$ and $\theta_2 = 30.88025^o$ with r.m.s. $= 0.00048^o \approx 8.6$ μrad.

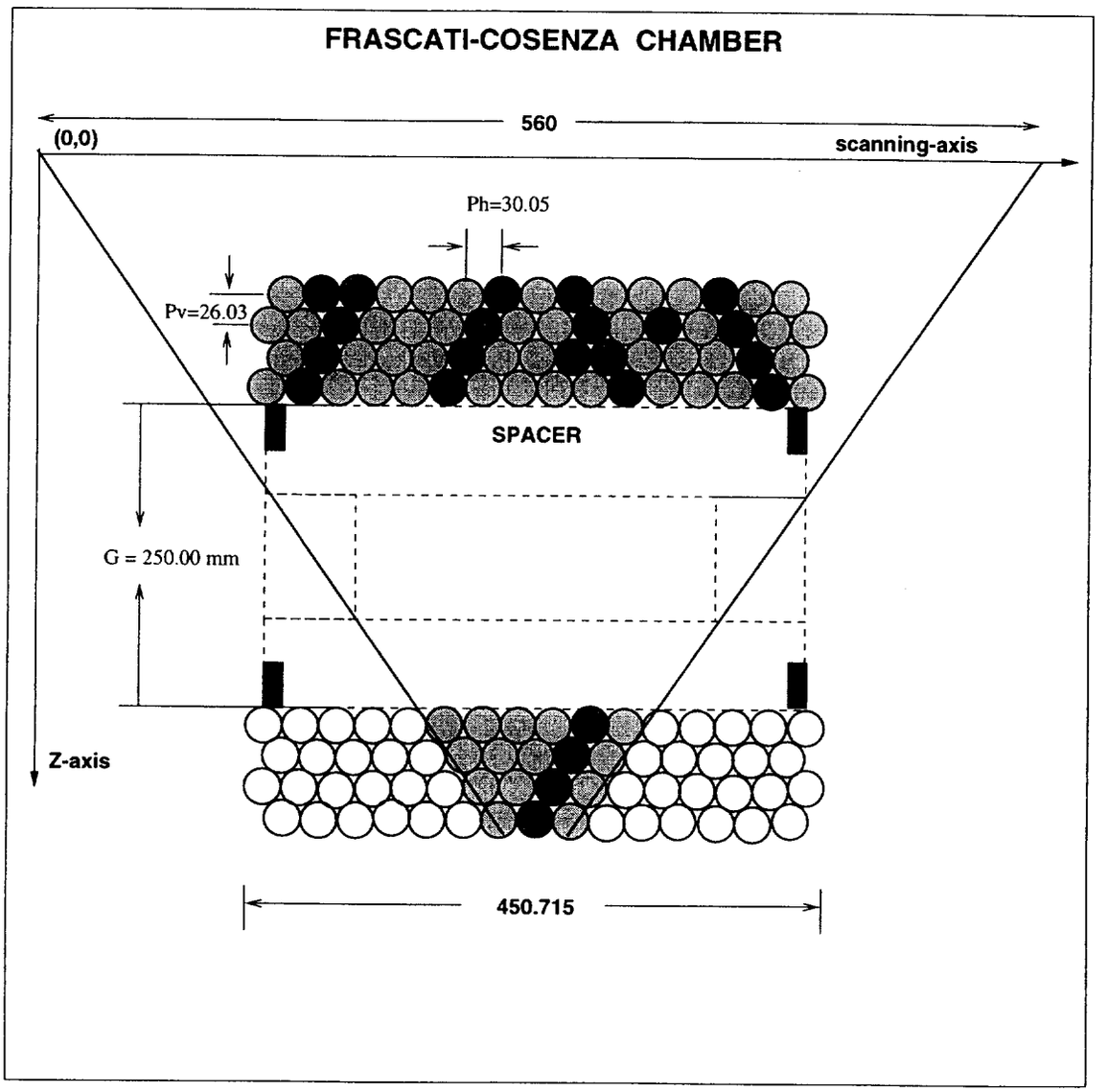

Figure 20: The intersection region of the two X-ray beams.

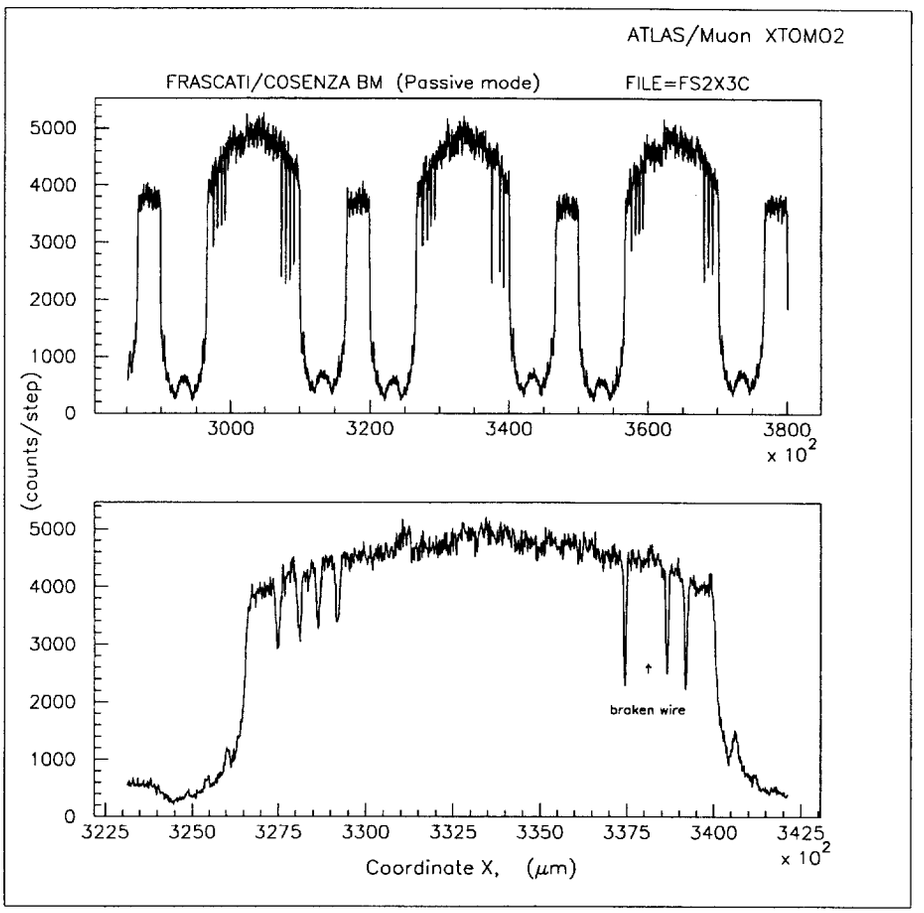

Figure 21: Passive mode: The counts per step of X-ray photons as a function of the scanner position (X-coordinate) for the 8-fold Cosenza-Frascati chamber. The bottom plot is an exploded view of the region where a broken wire is recognized.

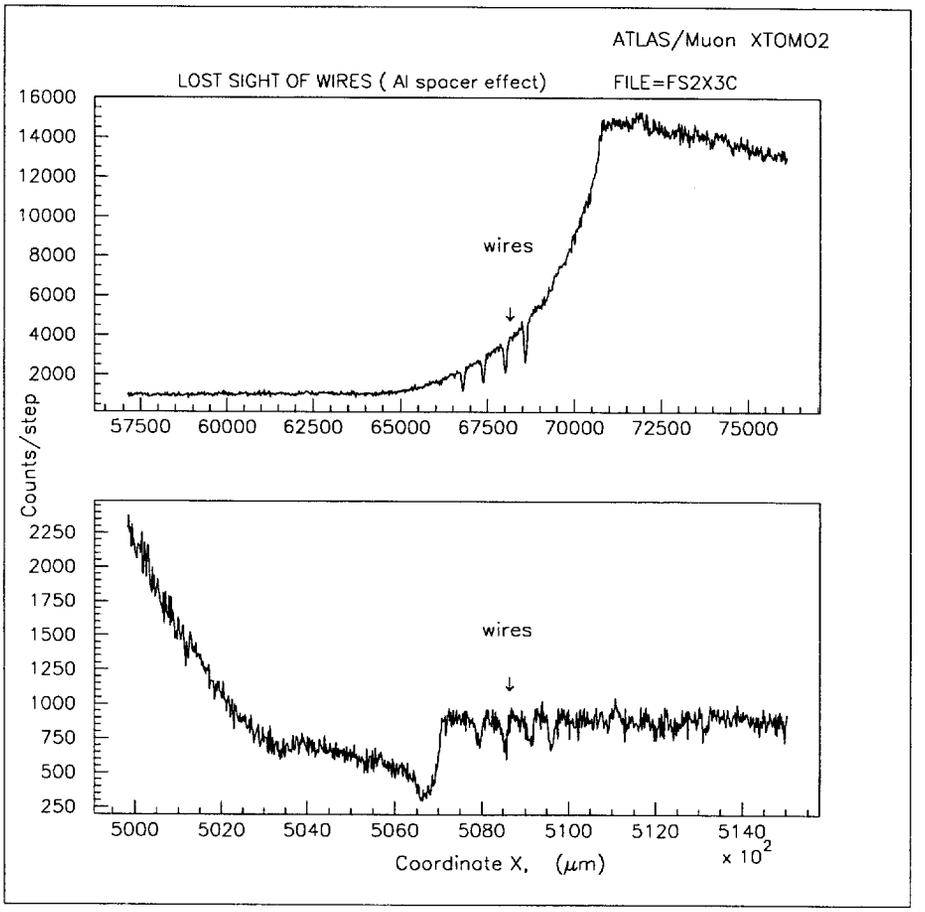

Figure 22: The counts per step as a function of the scanner position (X-coordinate) in the spacer region. The top and bottom plots show the effect of the spacer on the top and bottom multilayer wires respectively.

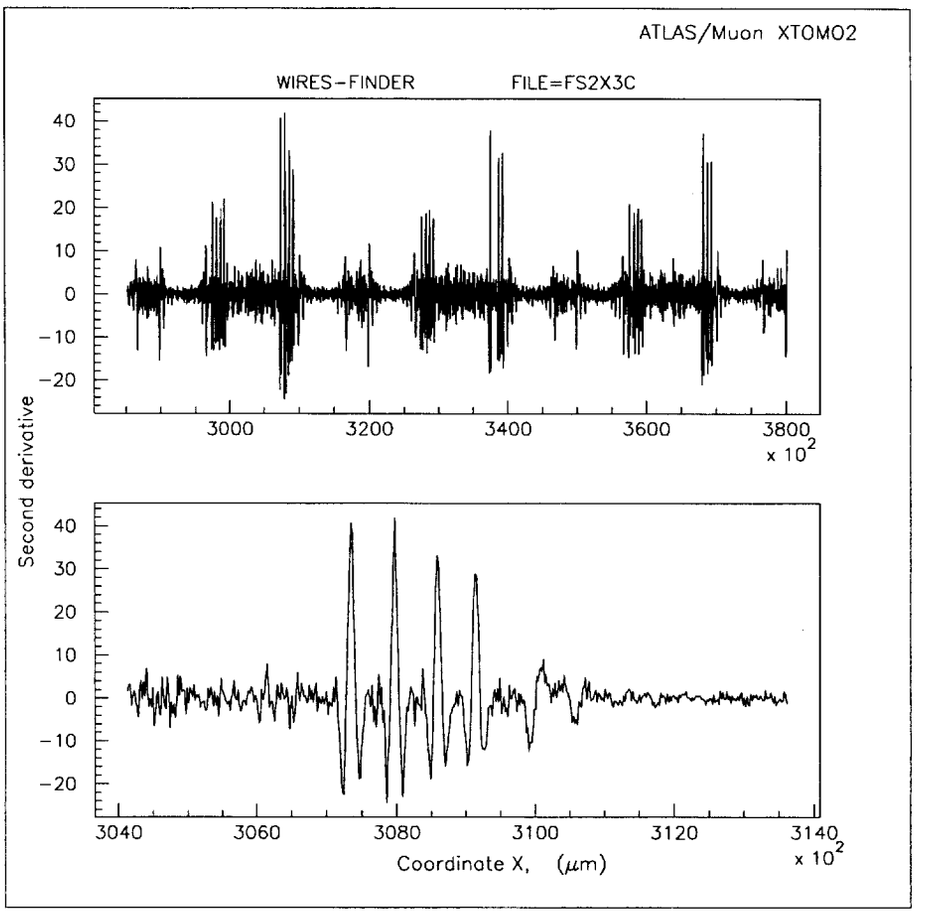

Figure 23: The second derivative as a function of the scanner position.

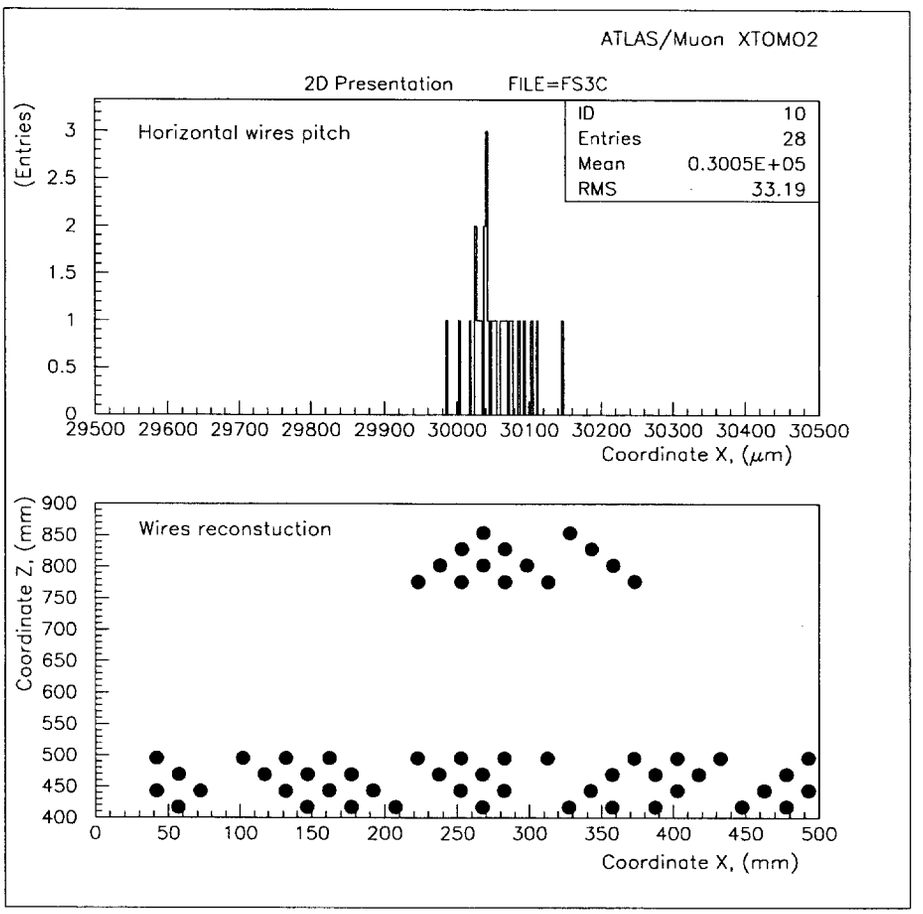

Figure 24: The distribution of the horizontal wire pitch (top) and the two-dimensional image reconstruction of the wire positions (bottom).

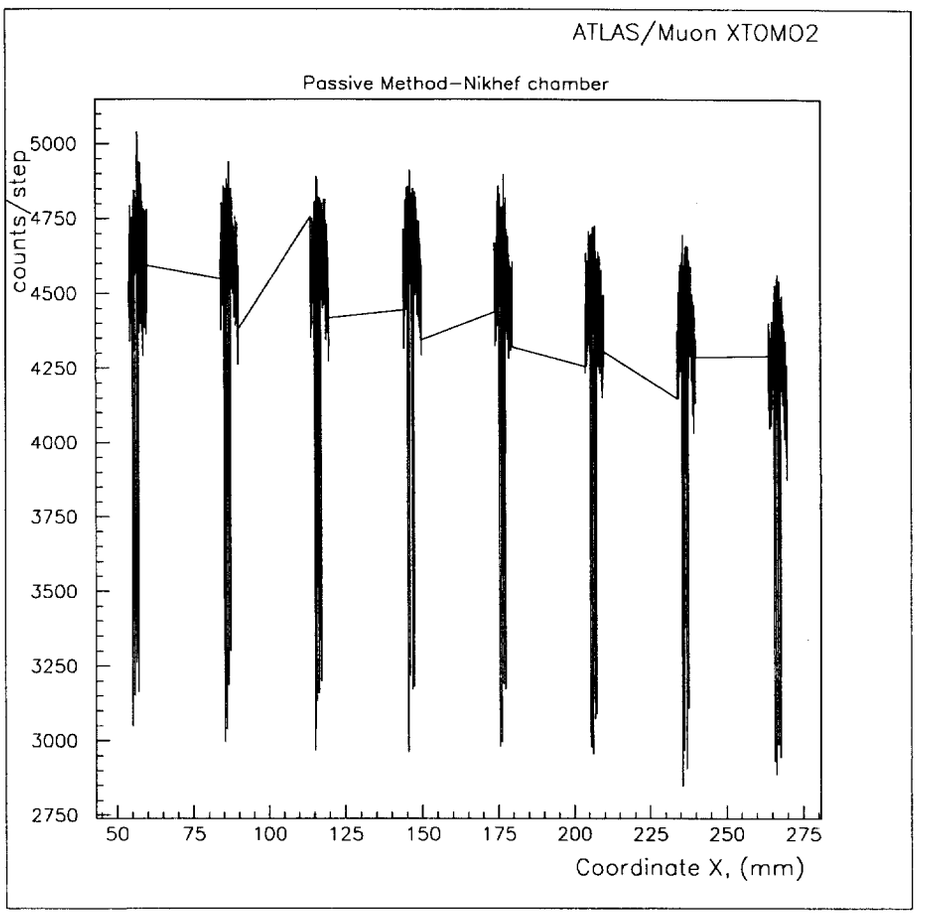

Figure 25: The shadow diagram for the Nikhef chamber: The counts per step of the X-ray photons, detected from a plastic scintillator, as a function of the scanner position .

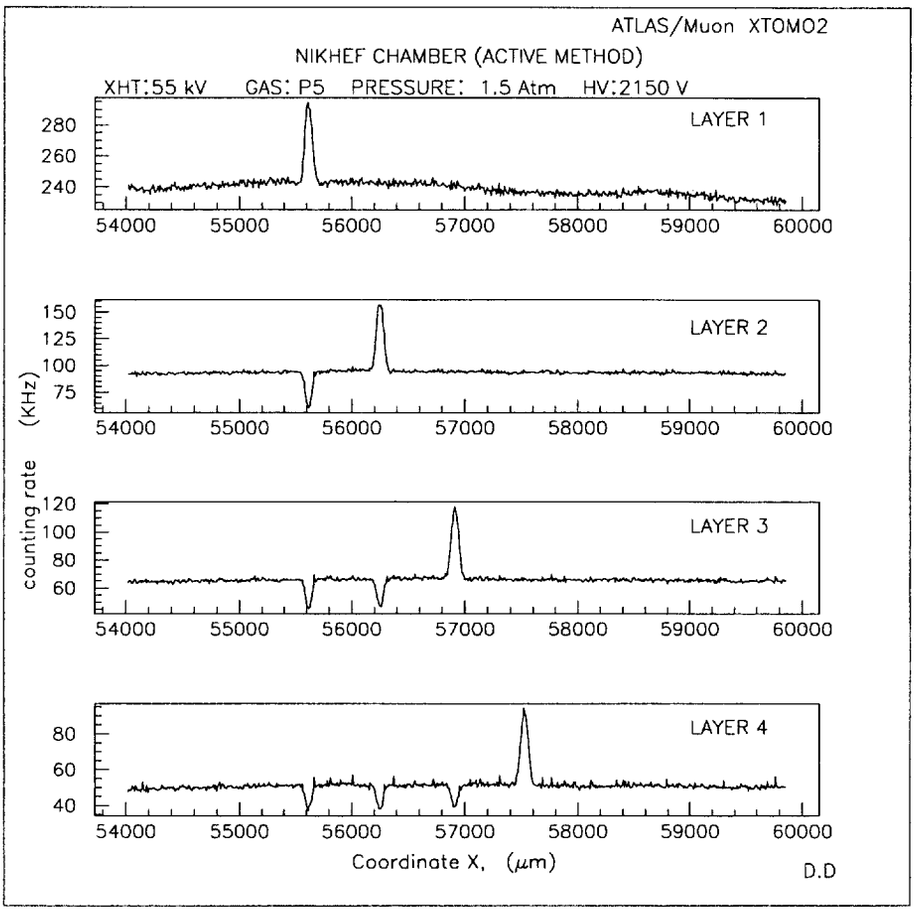

Figure 26: The wire sgnals (peaks) from four indivitual tubes belonging to same package. The peak correspond to the measured wire with the active mode and the dip(s) to the projected 'shadow' of the wire(s) of the top layer(s).

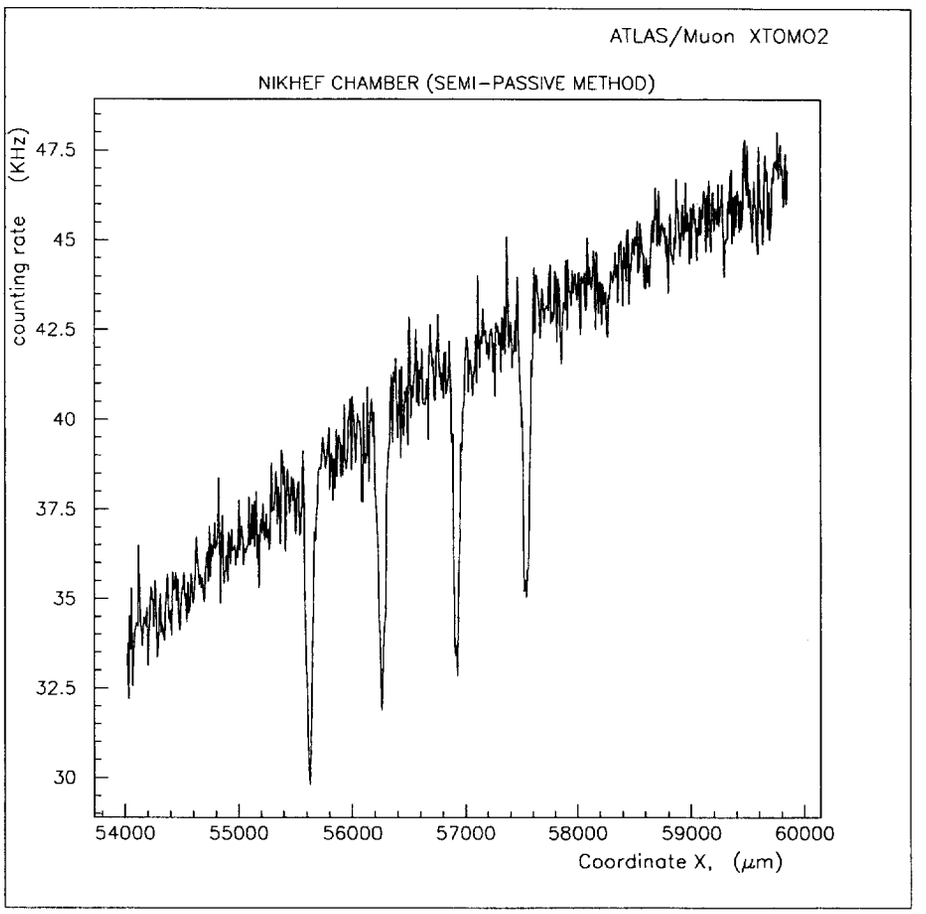

Figure 27: The shadow diagram for the semi-passive mode.

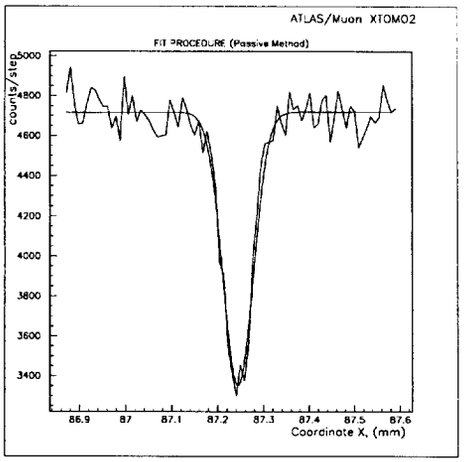

Figure 28: The fit of the wire signals (passive mode).

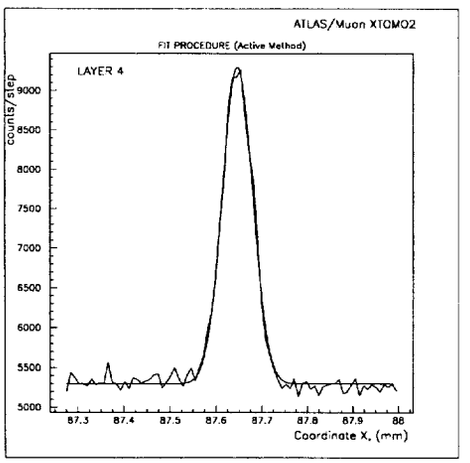

Figure 29: The fit of the wire signals (active mode).

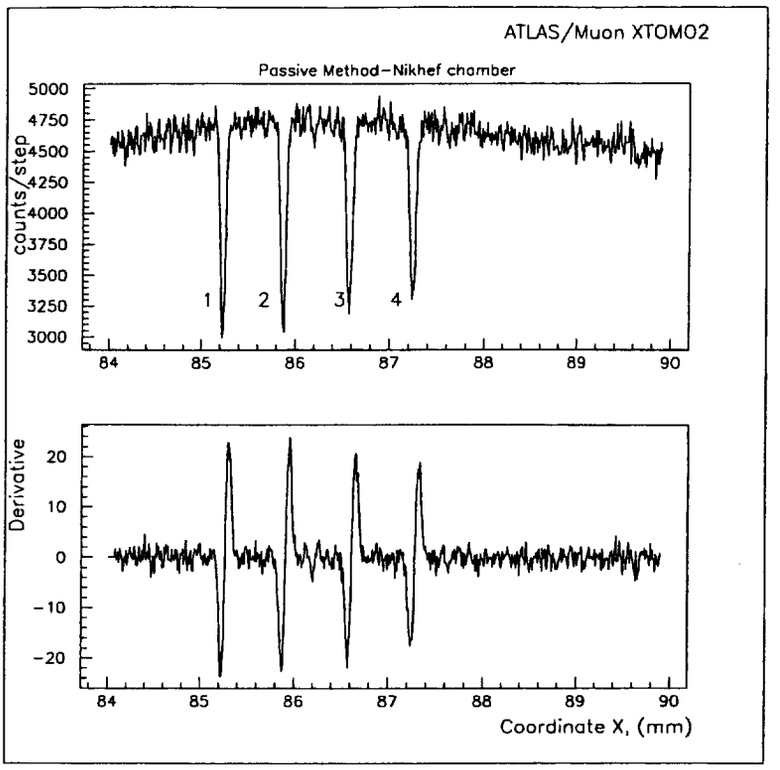

Figure 30: The first derivative of the counting rate as a function of the scanner position (passive mode).

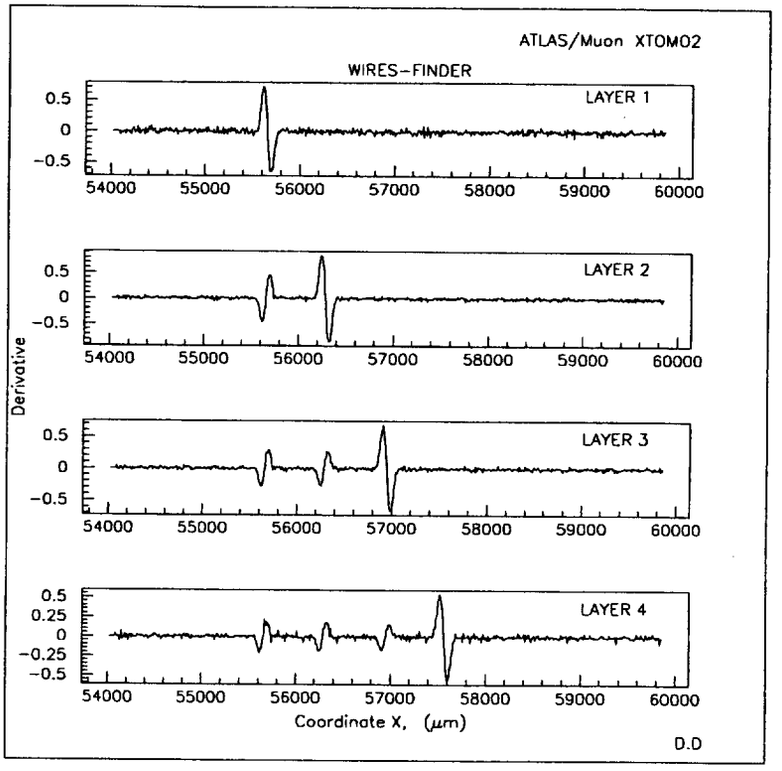

Figure 31: The first derivative of the counting rate as a function of the scanner position (active mode).

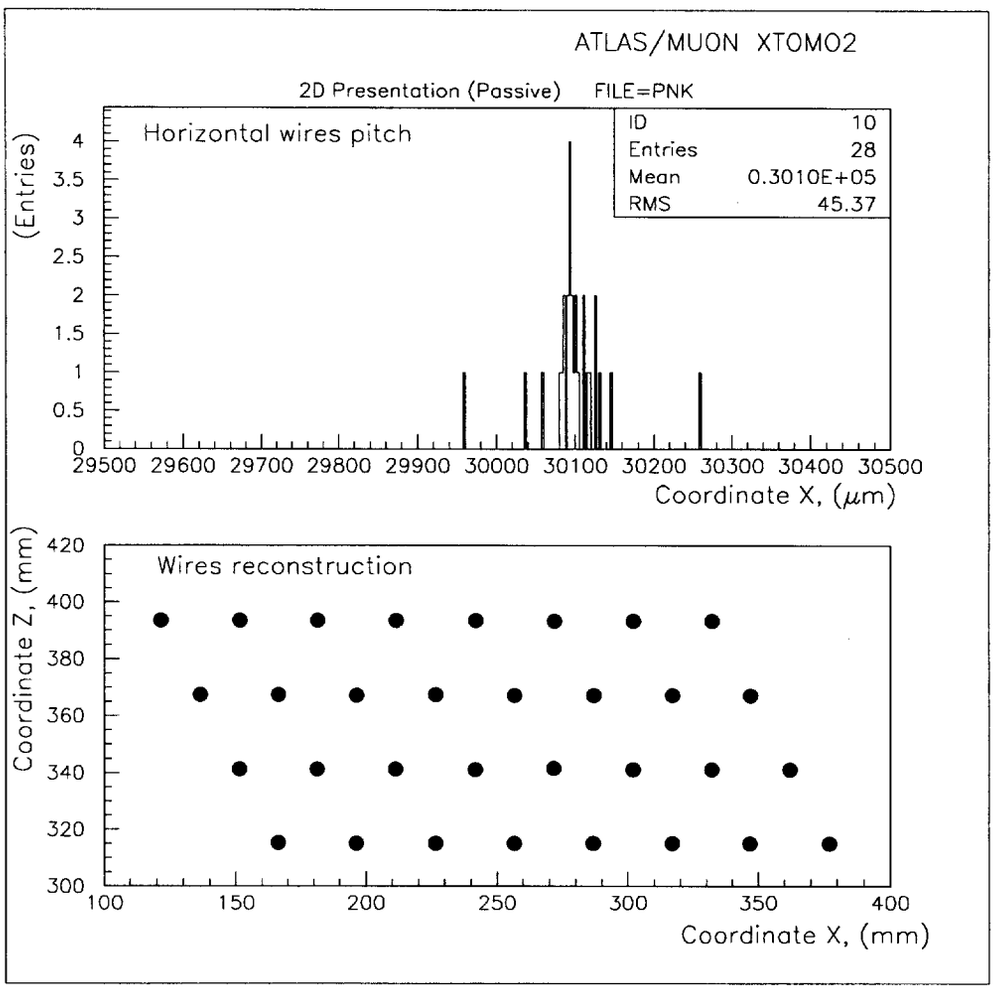

Figure 32: The distribution of the horizontal wire pitch (top) and the two-dimensional wire reconstruction (bottom) for the passive mode.

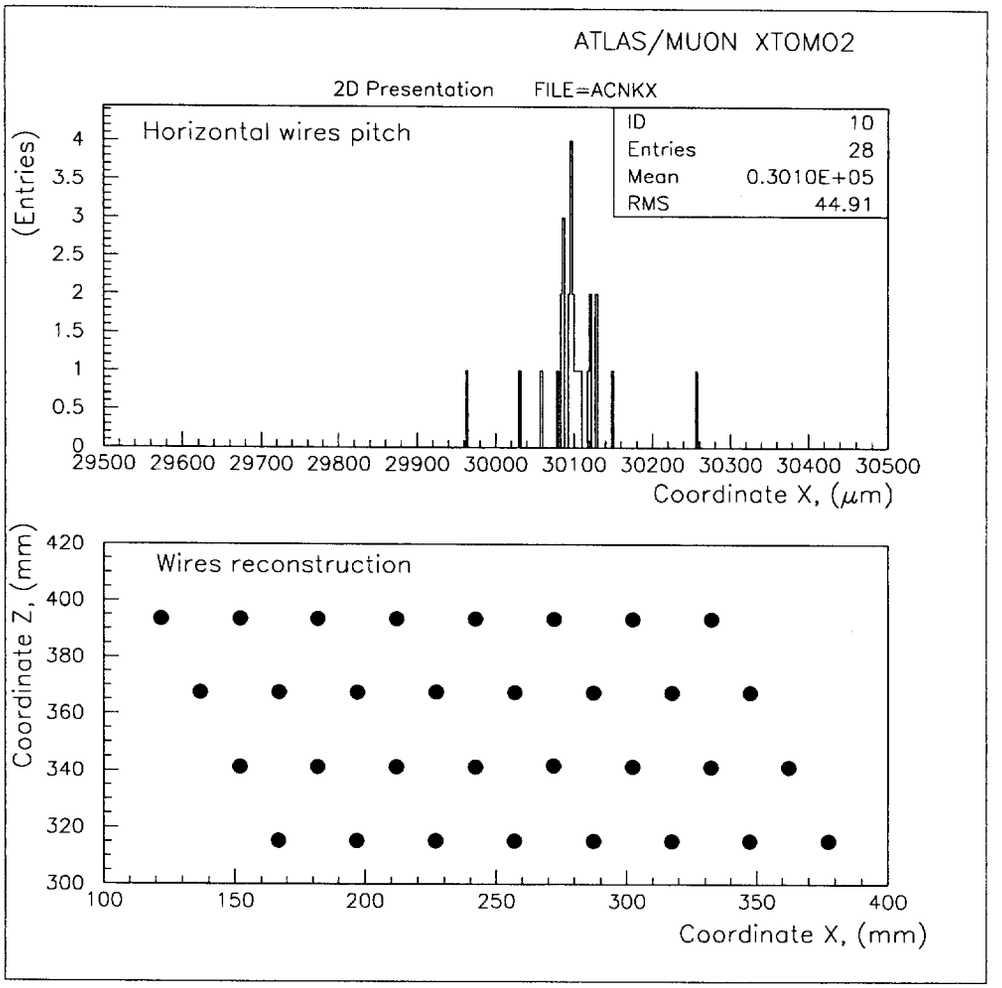

Figure 33: The distribution of the horizontal wire pitch (top) and the two-dimensional wire reconstruction (bottom) for the active mode.

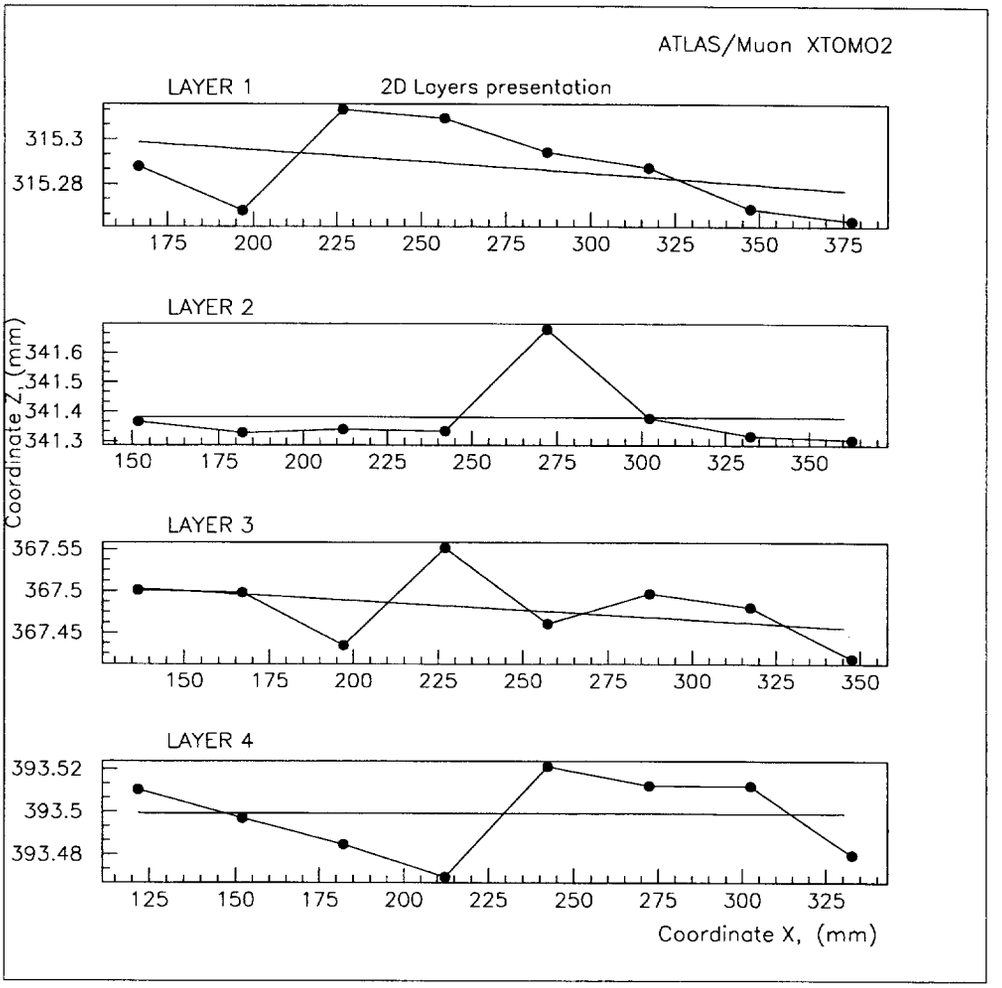

Figure 34: Two-dimensional wires reconstuction for the different layers.

APPENDIX 1: Tables

Table 1: The operating conditions of the XTOMO2 where the Nikhef chamber is scanned.

Scan. parameter	**Nikhef**		**Consenza-Frascati**
	Passive	Active	Passive
High Tension	45 kV	55 kV	45 kV
Current	15 mA	10 mA	15 mA
Collimator slit	40 μm	40 μm	40 μm
Scanning step	10 μm	10 μm	20 μm
Scanning angle	$\approx \pm 31^o$	$\approx \pm 31^o$	$\approx \pm 31^o$
Scanning program	stepped 2	stepped 2	flying 1
Disc. threshold	35 mV	30 mV	35 mV
Meas. time	100 ms	100 ms	100 ms
Gas	air	P5	air
Pressure	1 bar	1.5 bar	1 bar

Table 2: Two-dimensional reconstuction of the wire positions for the small Nikhef chamber.

NIkhef chamber							
Layer	Tube	Passive		Active		Error	
		x	z	x	z	Δx	Δz
		(mm)	(mm)	(mm)	(mm)	(μm)	(μm)
1	1	166.305	315.228	166.741	315.288	3	5
1	2	196.415	315.182	196.847	315.268	3	5
1	3	226.497	315.204	226.930	315.313	3	5
1	4	256.594	315.177	257.026	315.309	3	5
1	5	286.687	315.134	287.122	315.294	3	5
1	6	316.814	315.107	317.243	315.287	3	5
1	7	346.907	315.065	347.340	315.269	3	5
1	8	377.011	315.031	377.445	315.263	3	5
2	1	151.363	341.317	151.778	341.367	3	5
2	2	181.463	341.258	181.879	341.329	3	5
2	3	211.553	341.243	211.965	341.341	3	5
2	4	241.653	341.216	242.059	341.335	3	5
2	5	271.610	341.547	272.022	341.681	3	5
2	6	301.869	341.209	302.278	341.378	3	5
2	7	331.963	341.127	332.371	341.318	3	5
2	8	362.057	341.089	362.458	341.306	3	5
3	1	136.422	367.449	136.809	367.501	3	5
3	2	166.516	367.432	166.905	367.498	3	5
3	3	196.628	367.337	197.013	367.434	3	5
3	4	226.744	367.441	227.135	367.551	3	5
3	5	256.830	367.328	257.219	367.461	3	5
3	6	286.977	367.343	287.369	367.497	3	5
3	7	317.014	367.305	317.400	367.481	3	5
3	8	347.109	367.195	347.497	367.419	3	5
4	1	121.495	393.488	121.867	393.510	3	6
4	2	151.626	393.441	151.967	393.497	3	6
4	3	181.745	393.414	182.116	393.485	3	6
4	4	211.803	393.381	212.175	393.469	3	6
4	5	241.889	393.410	242.254	393.521	3	6
4	6	271.972	393.363	272.341	393.512	3	6
4	7	302.098	393.352	302.469	393.512	3	6
4	8	332.198	393.287	332.566	393.480	3	6

Table 3: Two-dimensional reconstuction of the wire positions for Frascati-Cosenza chamber.

Consenza-Fracati chamber					
Layer	Tube	x (mm)	z (mm)	Δx (mm)	Δz (mm)
1	1	56.904	417.146	0.004	0.007
1	2	1	1		
1	3	0	0		
1	4	147.048	417.239	0.004	0.007
1	5	177.112	417.249	0.004	0.007
1	6	207.259	417.305	0.004	0.007
1	7	0	0		
1	8	267.268	417.327	0.004	0.007
1	9	0	0		
1	10	327.386	417.381	0.004	0.007
1	11	357.389	417.415	0.004	0.007
1	12	387.466	417.447	0.004	0.007
1	13	1	1		
1	14	447.564	417.480	0.004	0.007
1	15	477.604	417.514	0.004	0.007
2	1	41.931	443.183	0.004	0.007
2	2	71.972	443.173	0.004	0.007
2	3	0	0		
2	4	132.056	443.196	0.004	0.007
2	5	162.159	443.279	0.004	0.007
2	6	192.219	443.308	0.004	0.007
2	7	0	0		
2	8	252.322	443.344	0.004	0.007
2	9	282.340	443.376	0.004	0.007
2	10	0	0		
2	11	342.466	443.410	0.004	0.007
2	12	1	1		
2	13	402.553	443.442	0.004	0.007
2	14	0	0		
2	15	462.699	443.539	0.004	0.007
2	16	492.739	443.544	0.004	0.007
3	1	57.023	469.165	0.004	0.007
3	2	0	0		
3	3	117.131	469.244	0.004	0.007
3	4	147.200	469.297	0.004	0.007
3	5	177.265	469.332	0.004	0.007
3	6	0	0		

3	7	237.385	469.368	0.004	0.007
3	8	267.373	469.379	0.004	0.007
3	9	1	1		
3	10	0	0		
3	11	357.566	469.474	0.004	0.007
3	12	387.592	469.484	0.004	0.007
3	13	417.641	469.532	0.004	
3	14	0	0		
3	15	477.753	469.576	0.004	0.007
4	1	42.024	495.204	0.004	0.007
4	2	0	0		
4	3	102.137	495.247	0.004	0.007
4	4	132.212	495.333	0.004	0.007
4	5	162.246	495.341	0.004	0.007
4	6	1	1		
4	7	222.325	495.398	0.003	0.007
4	8	252.419	495.431	0.004	0.007
4	9	282.447	495.430	0.004	0.007
4	10	312.498	495.469	0.004	0.007
4	11	0	0		
4	12	372.587	495.532	0.004	0.007
4	13	402.629	495.537	0.004	0.007
4	14	432.681	495.528	0.004	0.007
4	15	0	0		
4	16	492.764	495.628	0.004	0.007
5	7	222.989	776.358	0.006	0.011
5	8	253.074	776.433	0.006	0.011
5	9	283.114	776.438	0.006	0.011
5	10	313.157	776.465	0.006	0.011
5	11	0	0		
5	12	373.247	776.534	0.006	0.011
6	7	238.069	802.428	0.006	0.012
6	8	268.100	802.460	0.006	0.012
6	9	298.210	802.496	0.006	0.012
6	10	0	0		
6	11	358.255	802.556	0.006	0.012
7	8	253.173	828.459	0.006	0.012
7	9	283.199	828.477	0.006	0.012
7	10	0	0		
7	11	343.320	828.541	0.006	0.012
8	8	268.206	854.546	0.007	0.012
8	9	0	0		
8	10	328.316	854.547	0.007	0.012